Microthermometry of enargite-hosted fluid inclusions from the Lepanto, Philippines, high-sulfidation Cu-Au deposit using infrared microscopy

by

Daniel Peter Mancano

Submitted to the Faculty of the Graduate School of
The New Mexico Institute of Mining and Technology
in partial fufillment of the requirements for the degree of
Master of Science in Geochemistry

Department of Geoscience
1994

ABSTRACT

The spatial relation between porphyry and high-sulfidation epithermal deposits is particularly well revealed in the Mankayan mineral district of the northern Luzon, Philippines, where the Lepanto high-sulfidation Cu-Au deposit lies over and adjacent to the Far Southeast (FSE) porphyry Cu-Au deposit. Consequently, a study was undertaken to characterize the fluids responsible for epithermal mineralization in this environment. The ore stage at Lepanto consists of enargite-luzonite (Cu_3AsS_4), pyrite, tennantite-tetrahedrite, and chalcopyrite. Infrared petrography of the enargite reveals variable transparency, with growth banding and twinning visible in euhedral specimens. Two phase (liquid>vapor) fluid inclusions occur as primary and secondary types ranging from <1 to 80 micrometers in length, with tabular, cylindrical, or oval shapes. Homogenization temperatures (Th) of fluid inclusions in enargite from lateral (3.0 km) and vertical (0.5 km) extremes of the deposit show a cooling trend toward the northwest, away from the area over the porphyry deposit, with average Th ranging from 285°C (proximal) to 166°C (distal). Ice melting temperatures (Tm) were measured using a cycling technique, as ice was usually not visible in frozen inclusions. Apparent salinities range from 4.5 to 0.2 eq. wt. % NaCl, with samples from the margins of the deposit showing a general decrease in apparent salinity with lower Th. Secondary fluid inclusions in quartz phenocrysts tend to have a higher average homogenization temperature (281°C) compared to enargite hosted fluid inclusions (218°C) from the same locations. These secondary inclusions from the quartz phenocrysts also have generally lower apparent salinities. Several samples of pyrite are also transparent to IR radiation, and show internal features such as growth banding, and in one instance a two phase (liquid>vapor) fluid inclusion. This inclusion

yielded a salinity of 1.2 eq. wt. % NaCl. Radiometric age data supports a close temporal relationship between the enargite and porphyry mineralization. However, there is a large discrepancy in Th and apparent salinities between the enargite mineralization and the subjacent porphyry deposit, suggesting that the hot (>500°C) hypersaline magmatic brines did not directly ascend to the elevation of the enargite deposit. However, absorbtion of magmatic vapors into overlying meteoric water may have created the mineralizing fluid of the Lepanto deposit. As this liquid moved to the northwest along the Lepanto Fault, it was cooled and diluted by mixing with groundwater, resulting in enargite deposition.

ACKNOWLEGEMENTS

I thank the Lepanto Consolidated Mining company for permission to conduct this study, and the Lepanto mine staff for their support throughout this project. Special thanks to my committee members Andrew Campbell (Advisor), William Chavez Jr., and David Norman. Partial equipment funding was received from the National Science Foundation grant # EAR-9219744. Support is acknowledged from the New Mexico Tech Research Fund, The Geological Society of America, The Geological Survey of Japan, and the National Science Foundation Summer Institute in Japan. I also thank Jeff Hedenquist for his help and support throughout this project as well as for discussion and review of this paper.

Other personal thanks go out to Lepanto's La Guerta Barangay and their Tanduay Barangay nights with Dan Howmuch, The NMT Campus Police for Tom Z's six year-Geo-Cop fund, my girlfriend Anja for her patience while I was in the box (Ich hab' dich lieb!), and Jeff Hedenquist for trying to get me a job at the best sushi-joint in Tsukuba (Oishii des ne! Jeff San).

CONTENTS

APPENDICES

FIGURES

TABLES

INTRODUCTION

Epithermal, high-sulfidation deposits commonly have a spatial association with underlying porphyry Cu-Au ore bodies (Sillitoe, 1989). This spatial relation is particularly well revealed in the Mankayan mineral district of the northern Luzon, Philippines, where the Lepanto high-sulfidation Cu-Au deposit lies over, and adjacent to, the Far Southeast (FSE) porphyry Cu-Au deposit. Several other porphyry prospects and two epithermal low-sulfidation precious and base metal deposits are also present in the district (Garcia, 1991). This study examines the characteristics of the fluid responsible for the high-sulfidation epithermal mineralization, and provides constraints on the mineralization processes in this particular hydrothermal environment.

Since many ore minerals are opaque to normal light, most fluid inclusion studies have been restricted to analyzing transparent gangue minerals such as quartz and calcite. However, in most high-sulfidation deposits like Lepanto, most of the transparent minerals are late and do not represent the ore stage (Hedenquist et. al., 1994b). The ore stage at Lepanto is commonly dominated by the opaque mineral enargite (Cu_3AsS_4). However, since enargite may be transparent to infrared (IR) radiation (Campbell et al., 1984), an IR microscope was used to study fluid inclusions in enargite ore samples from Lepanto. This has allowed the direct measurement of the homogenization and ice melting temperatures of inclusion fluids associated with high sulfidation mineralization. Secondary fluid inclusions within igneous quartz phenocrysts from the host rocks were also measured to determine the relationship to the enargite.

GEOLOGY

The Lepanto high-sulfidation Cu-Au deposit is located in the Mankayan district, ~70 km northeast of Baguio, in northeast Luzon, Philippines (Fig. 1). The

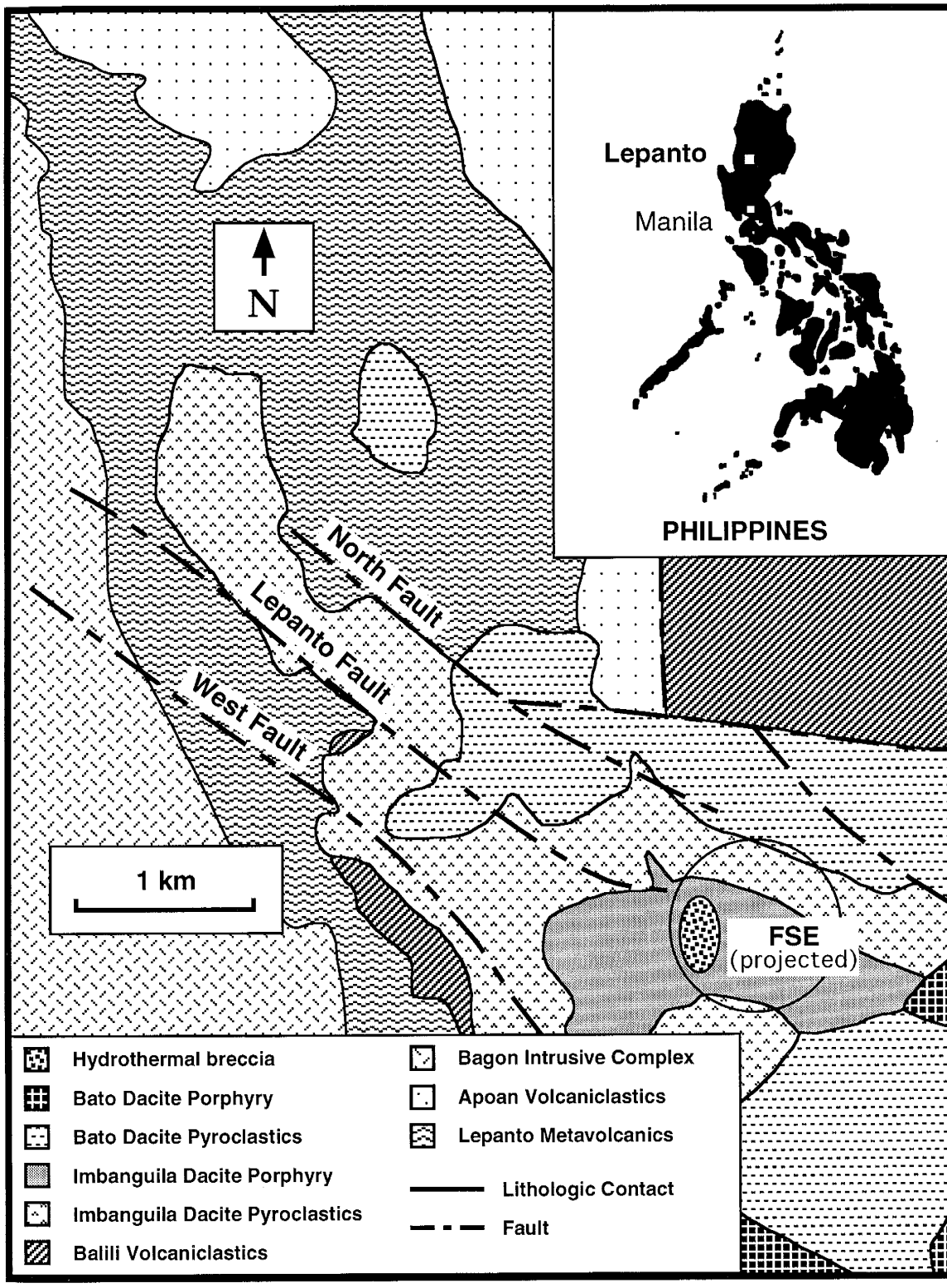

Figure 1. Plan view geologic map of the Lepanto, Philippines high-sulfidation Cu-Au deposit and FSE Cu-porphyry. Inset map depicts the mine location within the Philippine Islands.

major structural feature in the Mankayan district is the northwest-southeast Abra River Fault, which is the main branch of the Philippine Fault in the Luzon central cordillera (Ringenbach et al., 1990). A series of parallel, northwest trending normal faults, including the Lepanto fault, are associated in the Mankayan district with the Abra River Fault. The Lepanto fault hosts enargite-Au ore within a tectonic breccia zone 10-50 m wide, 100 m high, and over 2 km long (Garcia, 1991). On both sides of the fault, perpendicular tension fractures, called the Hanging-wall and Foot-wall Branch Veins, also contain ore. The Lepanto fault has a scissor-like, up-down motion which is greatest to the southeast (J.C. Cinco Jr., pers. comm., 1994).

The core of the Mankayan district consists of folded ophiolitic basement rocks in fault contact with younger rocks of the Bagon Tonalite (Garcia, 1991). The ophiolitic basement rocks are represented by the Cretaceous through Paleocene Lepanto Metavolcanics that consist of metamorphosed basaltic flows and andesitic volcanic rocks. The Lepanto unit is overlain to the east by the Miocene Balili Sequence (Fig. 2), which consists of volcaniclastic rocks, limestones, and shales. The Pliocene Imbanguila Dacite Porphyry and Pyroclastic deposits uncomformably overly the Balili and Lepanto units.

The southeast part of the district hosts the Far Southeast (FSE) Cu-Au quartz diorite porphyry deposit (Concepcion and Cinco, 1989), that is associated with quartz diorite stocks that intruded into the Balili Volcaniclastics. A hydrothermal breccia crosscuts the porphyry, and all of the overlying units, extending to the present surface.

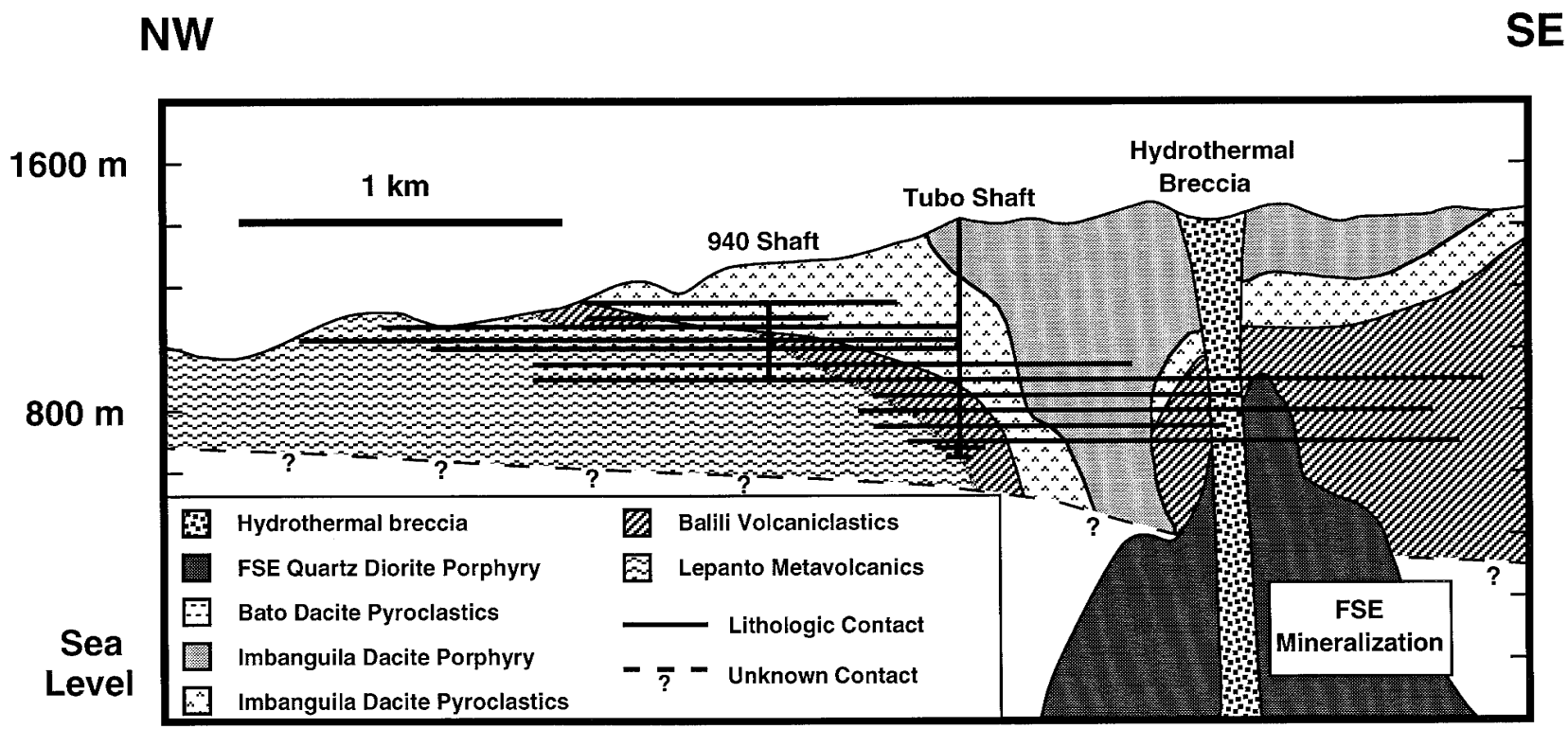

Figure 2. Cross section geologic map of the Lepanto, Philippines high-sulfidation Cu-Au deposit and FSE Cu-porphyry as seen along the Lepanto Fault. Major shafts and mine workings in the enargite ore body are also shown.

ALTERATION AND MINERALIZATION

Alteration

At Lepanto, the alteration distribution, like mineralization, is controlled by host rock permeability, unconformities, and fractures. An advanced argillic alteration assemblage is always present in the host rock adjacent to the enargite-bearing ore zones, with mineralogy and zonation typical of that noted for high-sulfidation deposits elsewhere (Steven and Ratté, 1960). The alteration progresses outward from veins and fractures into the host volcaniclastics and pyroclastics. A central zone of residual silica is formed by acid leaching (Hedenquist et al., 1994b), followed by alunite-kaolinite-pyrite to pyrophyllite-kaolinite-pyrite to illite-kaolinite-pyrite assemblages with distance from the ore. The alteration zones are narrower in the volcaniclastics; expand in the overlying permeable areas adjacent to the unconformity; and also extend for up to 30 meters into the overlying pyroclastics as a blanket (Gonzales, 1959). Depending on the host rock, the outermost alteration zone is either smectite-illite (pyroclastics) or chlorite-epidote-calcite (volcaniclastics) (Garcia, 1991). This advanced argillic alteration is indistinguishable from the advanced argillic cap of the underlying FSE porphyry where the two overlap. The deeper FSE alteration, below the advanced argillic cap, is composed of three zones enveloping each other away from the porphyritic intrusions. This zonation progresses outwards from potassic to illitic/chloritic, to propylitic alteration (Concepcion and Cinco, 1989), with illitic alteration commonly overprinting earlier alteration.

Dating of alteration minerals by Arribas et al. (1994) indicates contemporaneous ages for minerals intimately associated with the Lepanto high-sulfidation ore deposit (1.56 to 1.17 Ma $\pm$ 0.1 Ma for alunite) and Cu-Au

porphyry mineralization of the FSE (1.45 to 1.22 Ma $\pm$ 0.04 Ma for biotite and illite).

Mineralization

The Lepanto deposit contains three types of ore mineralization (Garcia, 1991): 1) the main ore body (MOB) is hosted by the Lepanto fault and consists of a tectonic breccia with enargite-luzonite occurring as both matrix and breccia clasts. A conjugate extension of this area is called the North-zero-A (NOA); 2) narrow (<10 cm wide) branch veins which are oblique to the MOB on both sides of the Lepanto Fault (Foot-wall and Hanging-wall Branch Veins); and 3) podiform/stratiform bodies that occur in between the overlying Imbanguila Dacite Pyroclastics and the Balili Volcaniclastics. These ore bodies vary in area from 10-300 m^2 and have a thickness of several centimeters to several meters. Highly permeable agglomeratic and laminated units that surround the unconformity and occur in other parts of the deposit also host stratiform mineralization.

Two stages of mineralization have been identified (Gonzales, 1959; Claveria and Hedenquist, 1994). Stage I consists of enargite-luzonite and euhedral to subhedral pyrite. Stage II commonly cuts stage I ore, and is dominated by tennantite-tetrahedrite, chalcopyrite, and anhedral pyrite with lesser occurrences of sphalerite, galena, marcasite, and minor enargite-luzonite. Most gold occurs in stage II as electrum (900 fine) and telluride minerals.

The Lepanto Consolidated Mining Company's 1992 annual report shows the following production values for the enargite ore body operations in 1992: Production tonnage totalling 1,023,731 dry metric tonnes (DMT) with head

grades of 1.197% copper, 2.1710 grams of gold per ton and 10.6923 grams of silver per ton.

PREVIOUS STUDIES

Early studies concentrated mainly on district geology, mineralization, and alteration (Evelend, 1905; Lehlbach, 1906; and Gonzalez, 1959). Recent studies (Garcia, 1991; Silitoe and Angeles, 1985; and Concepcion and Cinco, 1989) contain newer, revised concepts of the geology and exploration targets. More specialized research reviewed by Hedenquist and Arribas (1994) yields information on age dating, detailed paragenesis, sulfur isotopes, chemical variations in alunite, and fluid inclusion microthermometry of the enargite ore body (from the author) and FSE. Prior to the preliminary results of this study, the only published fluid inclusion data available was that from Concepcion and Cinco (1989) that contained data from the FSE Cu-porphyry.

INFRARED MICROSCOPE TECHNIQUES

Previous applications of infrared microscopy in the study of opaque minerals (eg. Campbell et al., 1984; Campbell and Robinson-Cook, 1987; Deen, 1990; and Richards, 1993) have shown the value of this technique to understanding metallogenic processes in hydrothermal ore deposits. The use of IR detectors to view internal features within opaque minerals is based on the principle that minerals either transmit or absorb various wavelengths of light depending on their electronic structure which is quantified as the band gap (Burns 1970). Minerals with band gaps greater than or equal to the wavelength of the visible spectrum transmit light and thus are translucent to the human eye. Conversely, some minerals (e.g. enargite, wolframite, and pyrite) with a band gap less than the visible spectrum are opaque to the human eye because the visible light is absorbed by electronic transitions. However, they do transmit the

lower energy, near-infrared light. The IR light which is transmitted through such a mineral is imaged by an IR sensitive camera and displayed on a television monitor.

Enargite was studied using an Olympus BHSM-IR microscope with specially coated, IR-enhancing optics. These include a 50X objective mounted as a substage condenser to optimize light transmission to the matching objective above. An Electrophysics IR camera sensitive to the near IR wavelength range of 0.8-2.2 micrometers is attached to the trinocular head assembly, and the camera connected to a television monitor and color video printer. Microthermometry was performed using a USGS-type gas-flow stage to record homogenization (Th) and ice melting (Tm) temperatures.

Conventional doubly polished thick sections were ground to 50-150 micrometer thickness for use on the fluid inclusion stage. The small diameter of conoscopic light (~200 micrometers) from the substage condenser allowed only very localized measurements in the thick sections. However, this containment of ambient light prevents any preferential IR absorption by the thermocouple in the heating stage. Measurement of H_2O, H_2O-CO_2, caffeine, sulfapyridine, and silver chloride standards with the IR scope indicates there is no preferential IR absorption from the transmitted light source.

FLUID INCLUSION PETROGRAPHY

Over a three month period of underground fieldwork, geological and mineralization relationships were established for the purpose of this study. In total, ~70 locations were sampled from lateral and vertical extremes of the enargite mineralization. Fifty thick sections were prepared, with ~30 sections exhibiting a high degree of IR transparency. Eighteen of the 30 thick sections contained fluid inclusions suitable for study.

Enargite

Infrared petrography of the enargite (Fig. 3a) reveals variable transparency, most likely governed by compositional heterogeneities and internal structural defects within the mineral (Campbell, 1991). Growth banding and twinning are also visible in euhedral specimens. Two phase (liquid>vapor) fluid inclusions (Fig. 3b) occur as primary and rare secondary types ranging from <1 to 80 micrometers in length, and are either tabular, cylindrical, or oval in shape. Since the majority of enargite mineralization is thought to occur in stage I of the mine's mineral paragenesis, the enargite-hosted fluid inclusion measurements likely correspond to this stage.

The resolution of the IR camera is not as good as a normal microscope, and thus only inclusions greater than five micrometers in length were measurable. Many fluid inclusions (mostly in secondary planes) were not measurable due to variable IR transparency and intra-inclusion opacity. These phenomena are probably created by compositional heteregeneities in the host mineral as well as the oblique orientation of the inclusions to the transmitted light path. Due to these factors, each thick section usually yielded less than five measurable fluid inclusions. The varying degree of IR transparency also caused difficulty in establishing whether an inclusion was primary. However, measurement of inclusions which were isolated or in growth zones consistently yielded the same values as neighboring inclusions with a questionable origin.

Since ice was not visible except for two occurrences, Tm values were measured using a cycling method described by Goldstein and Reynolds (1994). Tm was determined by heating the fluid inclusion in 0.1°C increments, followed by rapid cooling until the ice phase no longer regrows in the inclusion. Homogenization temperatures were also obtained by a cycling technique (Goldstein and Reynolds, 1994) due to the presence of thick, dark, inclusion

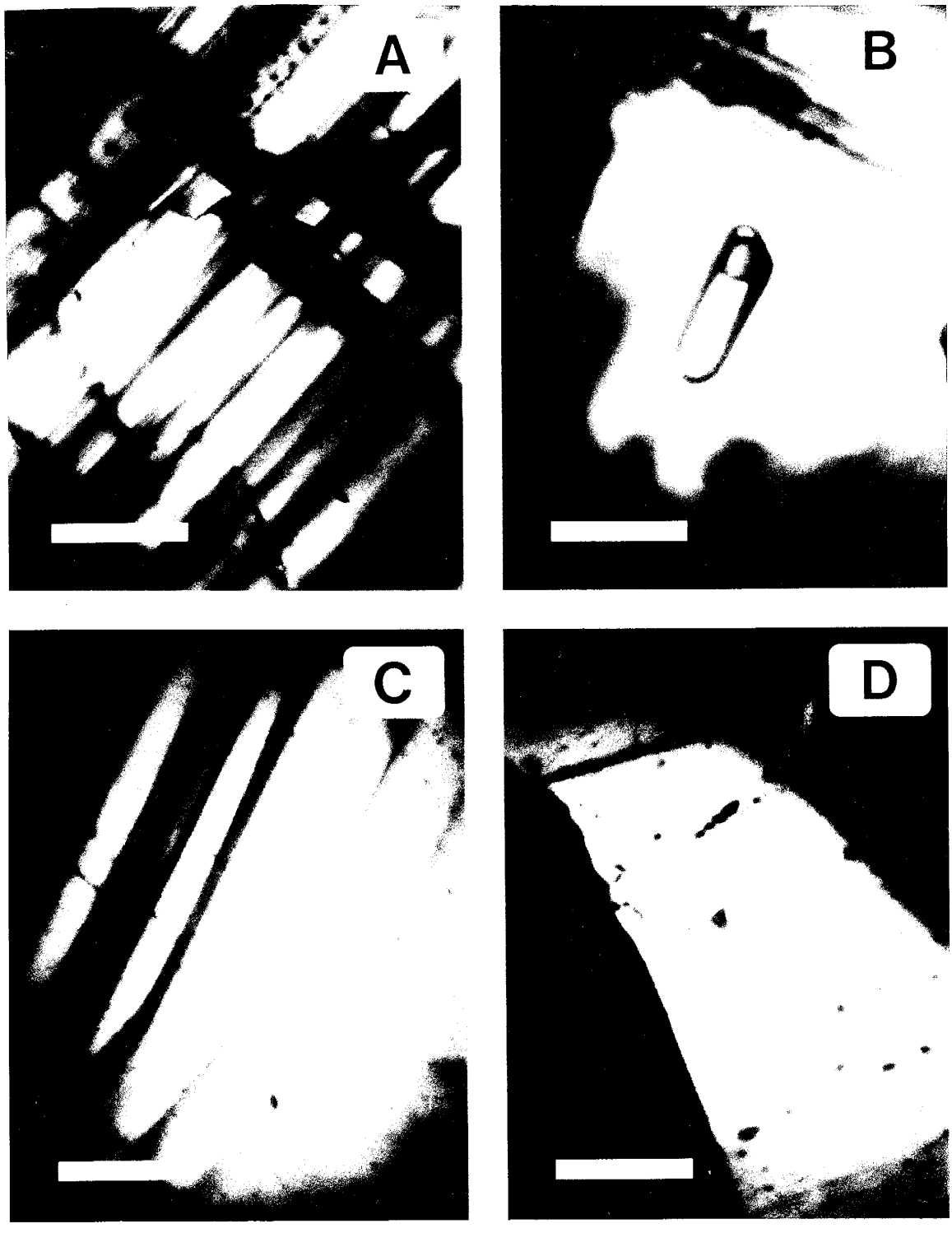

Figure 3. Infrared photomicrographs of enargite and pyrite. Scale bar in each photo equals 50 micrometers. a) Growth zones and twinning in enargite. b) Two-phase (liquid>vapor) fluid inclusion within enargite. c) Growth zones in pyrite. d) Two phase (liquid>vapor) fluid inclusion within pyrite.

borders that often obscured the vapor phase during the approach to homogenization. Th cycling is carried out by heating the fluid inclusion in 1.0°C increments and then lowering the temperature to see if the vapor phase either grows back to its original size, or abruptly nucleates (signifying Th is reached) upon cooling.

Two inclusions were analyzed for stretching during analysis of Th. These inclusions were cycled in 20°C increments up to Th+100°C, and also cycled in one step to Th+100°C. In both cases the Th was checked after each step, and no stretching was detected for either inclusion.

Quartz Phenocrysts

Quartz phenocrysts from the wall rock (mainly volcaniclastics) contain abundant secondary fluid inclusion planes which crosscut each other representing multiple events. Three types of inclusion assemblages were noted in order of decreasing abundance: 1) all liquid, all vapor, and variable liquid to vapor ratio inclusions occurring in the same plane (possibly representing two phase entrapment), 2) consistent liquid > vapor ratio inclusions, and 3) multi-phase inclusions containing liquid + vapor + NaCl $\pm$ an unknown phase. Quartz overgrowths were noted surrounding the phenocrysts as well as in open space fillings of the silicified host rock. Since the analysis of the quartz phenocrysts is being used as a comparison to the main enargite mineralization study, only secondary fluid inclusion planes containing consistent ratios of liquid plus vapor inclusions were measured in the interest of consistency and time.

Pyrite

Several samples of Lepanto pyrite are also transparent with the IR camera, showing similar growth banding (Fig. 3c) and in one instance a two

phase (liquid > vapor) fluid inclusion (Fig. 3d). This pyrite-hosted fluid inclusion has a Tm of -0.7°C (for an apparent salinity of 1.2 eq. wt. % NaCl). This is the first report of a microthermometry result for a pyrite-hosted fluid inclusion (Mancano and Campbell, 1994). However, upon heating, the sample became completely opaque before the homogenization temperature was reached. This heating phenomena has also been observed in some other IR-transparent minerals, and is caused by the temperature dependence of the band gap. As the temperature increases, the band gap decreases so that even the lower energy, near IR, is now absorbed.

RESULTS AND DISCUSSION

The Th and Tm values of 151 fluid inclusions in enargite, one fluid inclusion in pyrite, and 52 secondary fluid inclusions in quartz phenocrysts from the wall rock were obtained and are presented in table 1 with the number (n), range, standard deviation (s), and average ($\bar{x}$) of the Th and Tm data sets. The sample suite consists of 21 locations chosen to represent the spatial range of enargite mineralization, including the vertical and lateral extremes of the deposit. Enargite samples from about 40 other locations were not sufficiently IR transparent to use for this fluid inclusion study. There are 15 sample locations with enargite only, three locations with quartz phenocrysts only, two locations with enargite+quartz phenocrysts from the same sample, and one location with quartz+pyrite from the same sample. Whenever possible, each mineral at every sample location had ~10 inclusions measured for Th and Tm.

Th variation

A geologic reconstruction of the area shows that the paleosurface was ≤500 meters above the present surface, and also had the same slope. Because

Table 1. Data summary of fluid inclusions from Lepanto, Philippines.

Sample #	Location	Mineral	Th (C°)				Tm (C°)			
			n	range	s	$\bar{x}$	n	range	s	$\bar{x}$
U.85.21	140 RZ 3 (592 lv)	Enargite	4	281-294	6	285	10	-1.1 to -2.6	0.5	-1.9
4.3.2	95 T (1030 lv)	Enargite	9	185-219	14	207	10	-1.1 to -2.3	0.5	-1.8
4.3.1	50 M 5 (1030 lv)	Enargite	7	175-232	23	194	10	-0.1 to -2.2	0.6	-1.2
4.3.1	50 M 5 (1030 lv)	Quartz	5	177-233	25	205	5	-1.0 to -1.7	0.3	-1.2
4.2.1	120 S (1030 lv)	Enargite	12	177-237	18	224	10	-1.2 to -2.0	0.3	-1.7
3.25.4	135 EZ XCS (850 lv)	Enargite	8	183-252	28	220	11	-0.8 to -1.9	0.3	-1.3
3.25.4	135 EZ XCS (850 lv)	Quartz	17	289-363	22	310	10	-0.1 to -0.8	0.3	-0.4
3.19.1	140 GZ (680 lv)	Quartz	10	242-351	45	300	10	-0.2 to -0.9	0.2	-0.7
3.17.1	175 CZ (900 lv)	Pyrite	-	-	-	-	1	-0.7	-	-0.7
3.17.1	175 CZ (900 lv)	Quartz	13	253-307	16	283	10	-0.2 to -2.5	0.9	-1.7
3.6.5	165 O (1200 lv)	Quartz	7	208-273	25	231	5	-0.2 to -1.1	0.3	-0.6
3.6.3	50 P, Q 2 (1000 lv)	Enargite	9	197-245	15	231	10	-0.4 to -2.0	0.5	-1.3
3.6.2	125 EZ 3 (950 lv)	Enargite	7	240-254	4	248	10	-1.1 to -1.5	0.2	-1.3
2.19.3	135 N1 (1100 lv)	Enargite	11	187-241	14	209	11	-0.8 to -2.3	0.5	-1.5
2.19.2	125 BZ 1 (700 lv)	Enargite	7	187-223	11	201	10	-0.5 to -1.7	0.4	-1.0
2.18.2	20 C (1000 lv)	Enargite	10	173-214	12	198	10	-0.5 to -2.2	0.7	-1.4
2.13.2	185 EZ (900 lv)	Enargite	5	175-245	31	206	6	-0.4 to -1.8	0.5	-1.2
2.12.1	140 GZ (700 lv)	Enargite	8	168-259	31	230	10	-0.3 to -1.7	0.4	-1.0
2.9.2	45 P 4 (950 lv)	Enargite	9	193-238	14	225	10	-0.8 to -2.7	0.5	-1.7
2.8.4	50 J 4 (1070 lv)	Enargite	1	207.0	-	207	1	-1.3	-	-1.3
2.6.4	(-)10 CW 3 (1030 lv)	Enargite	6	151-196	16	166	5	-0.9 to -1.2	0.1	-1.0
2.5.2	70 N 3 (1030 lv)	Enargite	-	-	-	-	1	-1.7	-	-1.7
2.2.2	165 IZ 1 (950 lv)	Enargite	8	233-267	10	249	10	-1.2 to -2.0	0.3	-1.6

of this small amount of overburden, pressure corrections were not necessary for the fluid inclusion data.

The average Th of all enargite-hosted fluid inclusions is 218°C, with a range of 151°C to 294°C (Table 1). The average Th values of enargite-hosted fluid inclusions at each sample location decrease laterally from the southeast to the northwest, along the trend of the Lepanto Fault, from 285°C to 166°C, respectively (Fig. 4). Fluid inclusions from enargite within the Hanging-wall and Foot-wall Branch Veins also show a decrease in Th with distance from the Lepanto fault. The motion along the Lepanto Fault, with the northeast side (hanging-wall) upthrown relative to the Foot-wall Branch Veins, is also reflected in the Th values of the enargite. This is represented by higher Th values in the Hanging-wall Branch Veins occurring at the same elevation as lower Th values in the Lepanto fault enargite. In general, the average Th values for secondary inclusions from quartz phenocrysts also show a northwest trend in cooling, from 310°C to 205°C.

Th-Tm variation

The averages of Th and Tm data for each sample location are shown in Fig. 5, and the individual Th and Tm data are plotted in figure 6. Figures 5 and 6 have Th plotted as equivalent enthalpy.

Enargite and quartz phenocrysts

A comparison of average Tm versus enthalpy shows the enargite-hosted fluid inclusions having an average Tm generally decreasing (-1.9°C to -1.0°C) with decreasing average Th (285°C to 166°C, respectively). The quartz-hosted secondary fluid inclusions have similar to higher average Th (310°C to 205°C), but similar to lower average Tm (ranging from -0.4°C to -1.2°C, respectively)

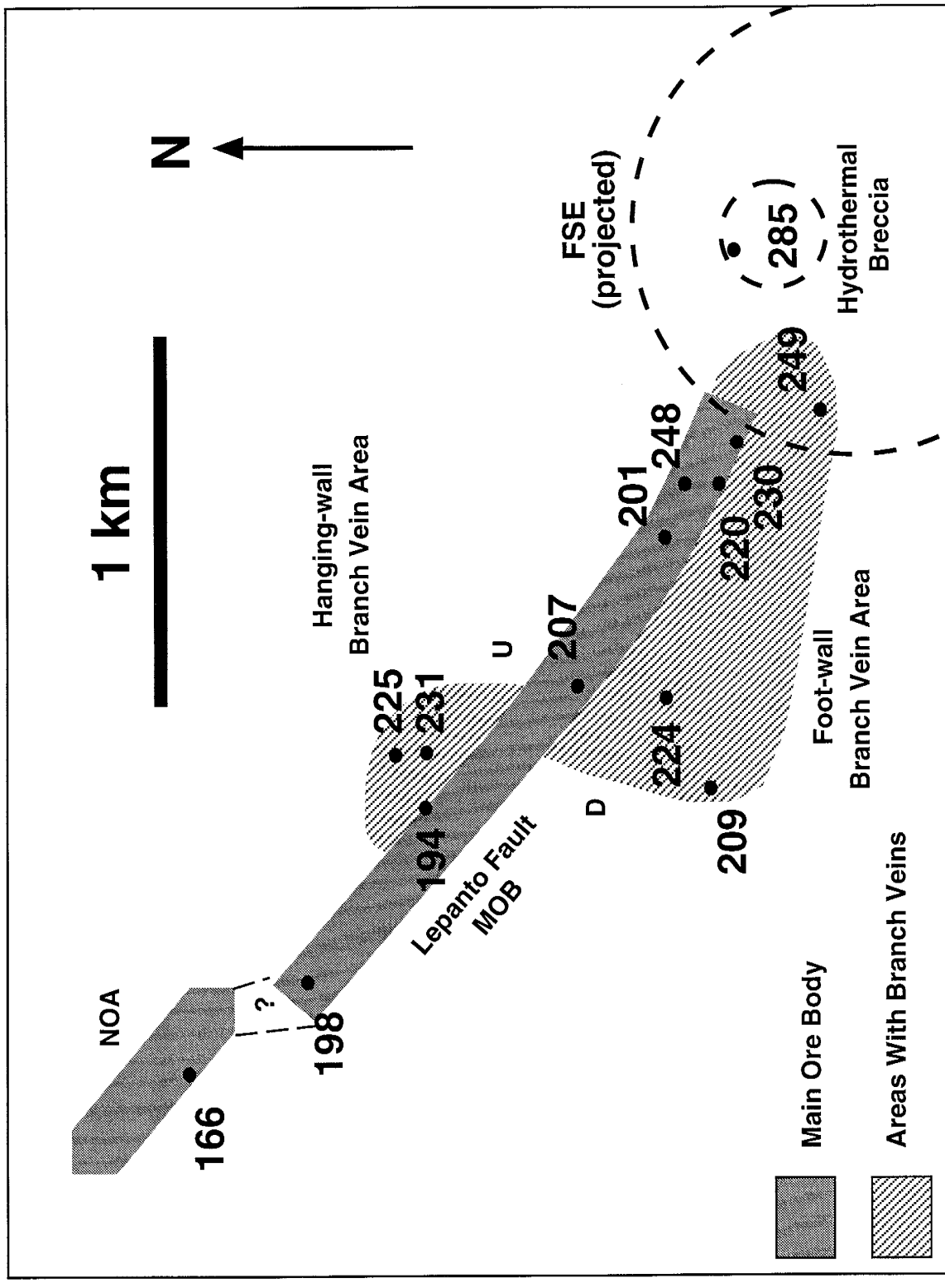

Figure 4. Plan view map of average Th variation in enargite-hosted fluid inclusions. Note the general SE to the NW cooling trend along the Lepanto Fault as well as outward through the Branch Veins.

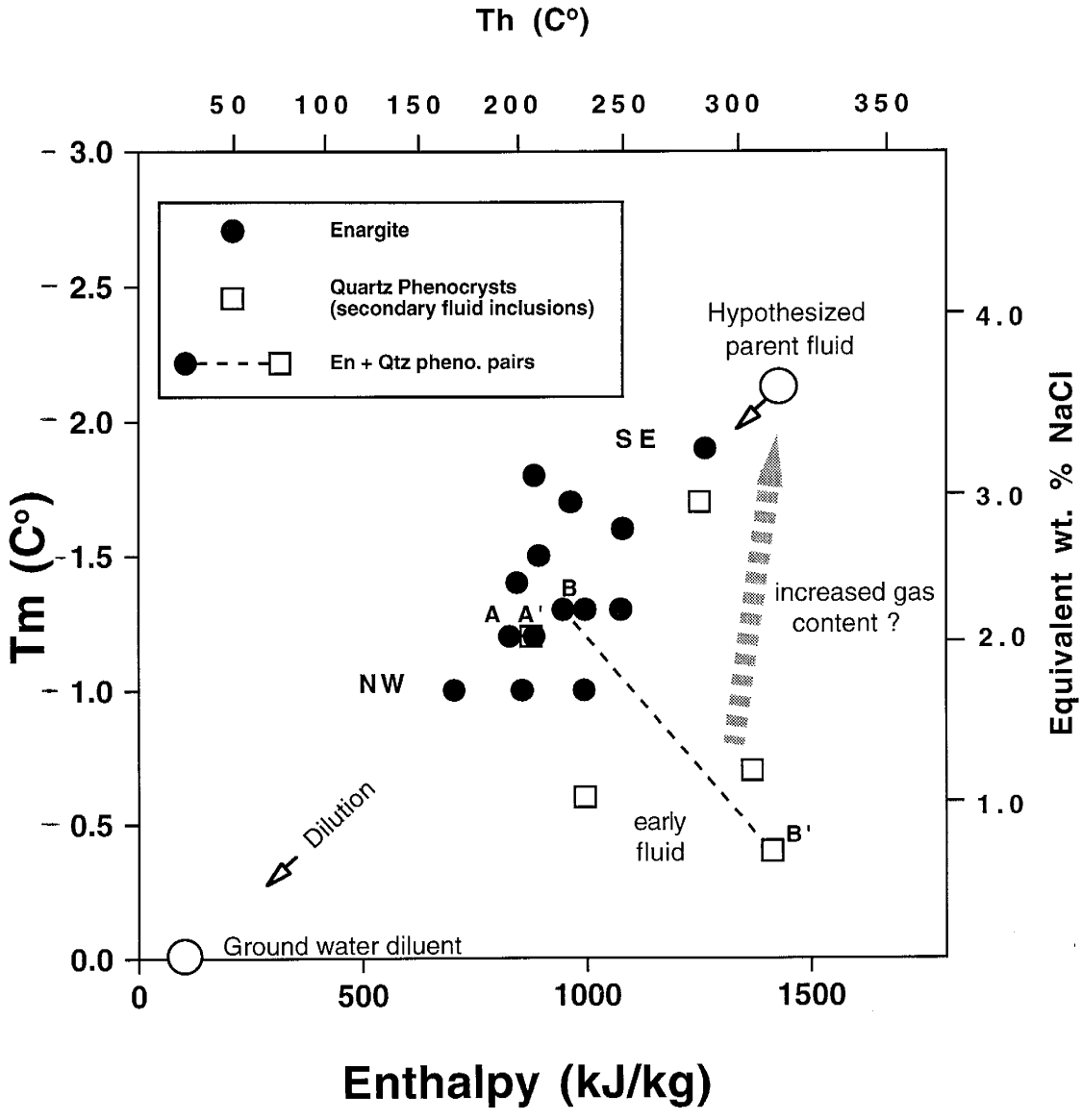

Figure 5. Average fluid inclusion data from Lepanto, Philippines. Tm is plotted vs. equivalent enthalpy and shows a cooling and dilution of enargite depositing fluids. This trend projects toward the composition of local groundwater.

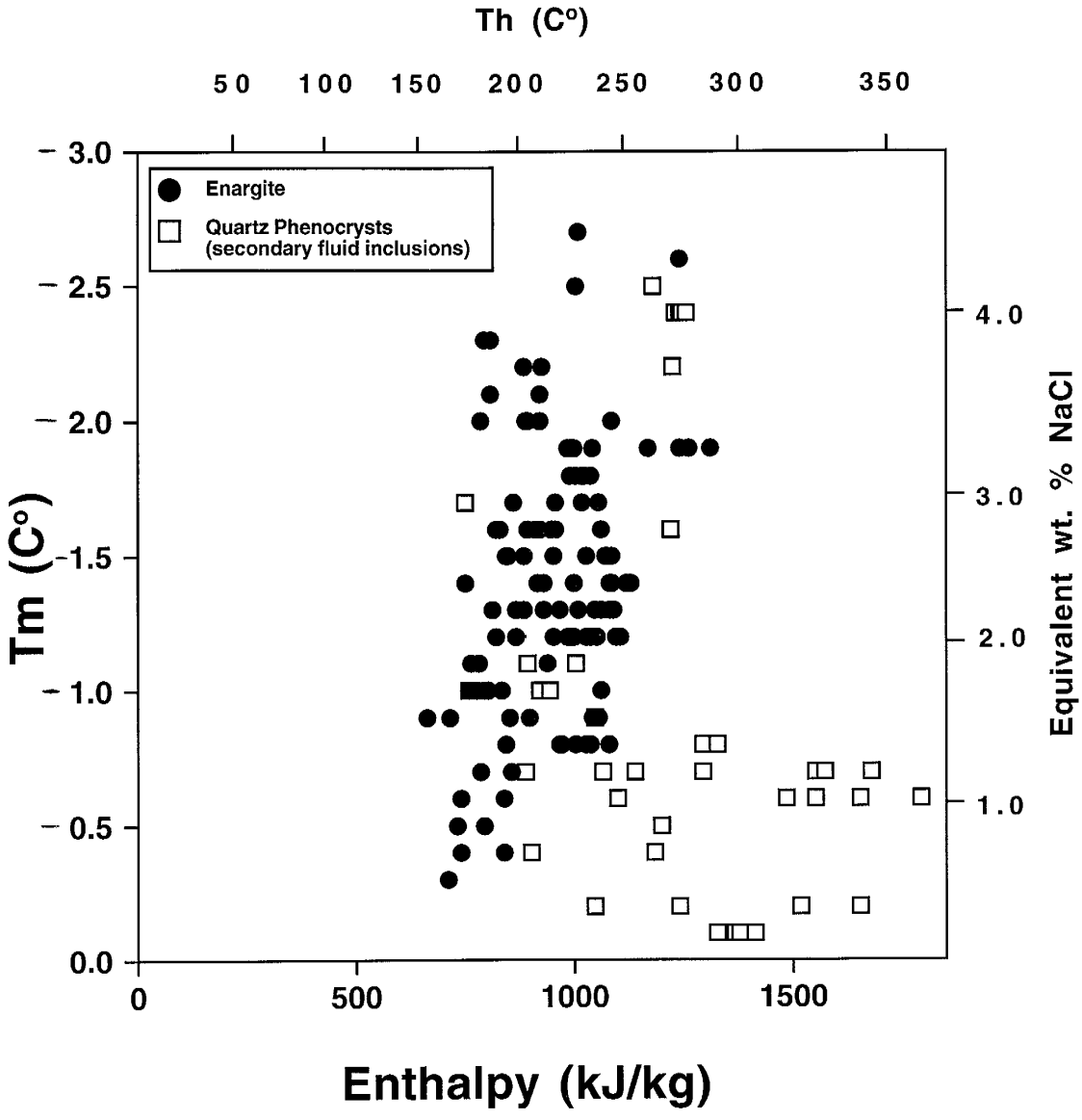

Figure 6. Individual fluid inclusion data from Lepanto, Philippines. Tm is plotted vs. equivalent enthalpy.

with no spatial trends in Tm. A comparison of fluid inclusions from enargite and quartz phenocrysts of the same sample shows two different results. One sample (sample# 4.3.1) has very similar Th and apparent salinity values for inclusions in the enargite and quartz phenocrysts (194°C and 2.1 eq. wt. % NaCl, versus 205°C and 2.1 eq. wt. % NaCl, respectively). In contrast, the other sample (sample# 3.25.4) has a large difference between the two sets of inclusions (220°C and 2.2 eq. wt. % NaCl, versus 310°C and 0.7 eq. wt. % NaCl, respectively). The latter intra-sample variance, along with the difference between the enargite and quartz phenocryst data sets, shows the value of measuring data directly from the ore stage as opposed to only relying on inclusions in surrounding gangue minerals.

Based on the values and occurrence of quartz phenocryst-hosted fluid inclusions, it is argued that the quartz phenocrysts trapped secondary inclusions of an early, pre-enargite, high-temperature and low-salinity fluid as well as the later enargite-depositing fluid. The lack of the former fluid type in the enargite-hosted fluid inclusions suggests enargite was deposited from a later distinct fluid, with some of this fluid occurring as secondary inclusions in some quartz phenocrysts.

Pyrite

The one pyrite inclusion (Sample# 3.17.1) yielded a salinity of 1.2 wt. % NaCl with a Th > 120°C. The Th was unable to be measured due to equipment limitations (see discussion above).

FSE porphyry quartz veins

There is a clear distinction between the low Th-high Tm (low salinity) epithermal fluid inclusions within the quartz and enargite samples and the high

Th-low Tm (high salinity) Cu-porphyry hosted inclusions referred to by Concepcion and Cinco (1989). The Cu-porphyry fluid inclusions have Th values of approximately 550°C and hypersaline salinities around 50 eq. wt % NaCl, both typical of the porphyry environment and distinct from the results presented here for the overlying Lepanto epithermal deposit. The porphyry, fluid inclusion values are also consistent with the FSE quartz values of >620°C and 68 eq. wt. % NaCl found by the author (Appendix C).

Fluid evolution

The trend of enargite-depositing fluids (Fig. 7) indicates cooling and dilution with increasing distance from the area of the FSE porphyry. An enthalpy conversion (Haar et al., 1984) was used for the Th data since mixing lines are straight in terms of Tm-derived solute concentrations versus heat content. Using the averages of the fluid inclusion data, the mixing trend in figure 5 projects to the composition of local groundwater (i.e., 20°C at 0.0 eq. wt. % NaCl), suggesting that as the hydrothermal fluid ascended and flowed laterally to the northwest, it was increasingly diluted by groundwater. A slightly different interpretation can be made by plotting the individual fluid inclusion data (Figure 6). This plot shows a similar pattern of dilution with lateral flow, though by hotter, steam-heated ground waters similar to the pattern for the Creede, Colorado, Ag-base metal low-sulfidation epithermal deposit (Hayba, 1984).

Radiometric age data (Arribas et al., 1994) supports a contemporaneous relationship between the enargite and porphyry mineralization. However, the lack of high-salinity, high-temperature inclusions in enargite samples bordering the upper limit of Cu-porphyry mineralization suggests that enargite mineralization did not directly involve the hot, hypersaline porphyry brines. It is likely that these dense brines did not ascend to the elevation at which enargite

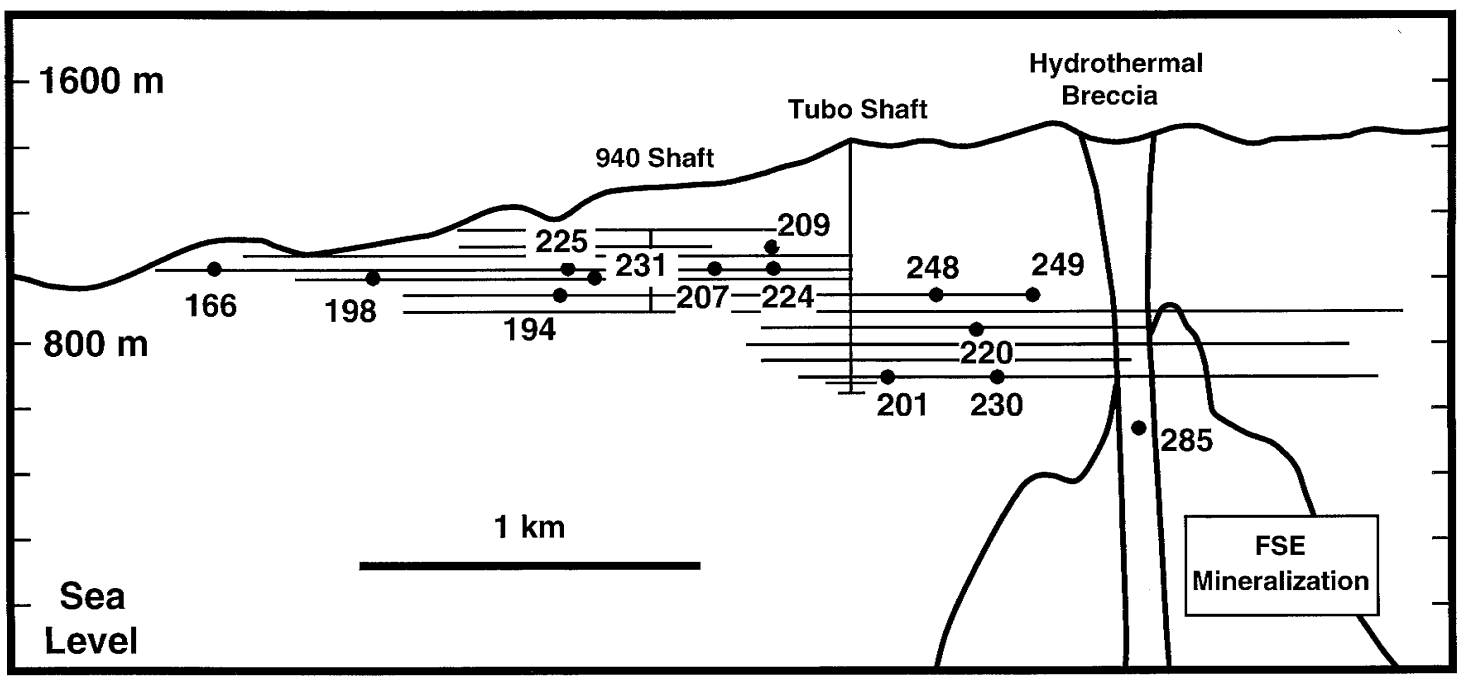

Figure 7. Cross sectional map of average Th variation in enargite-hosted fluid inclusions. Note the decrease in Th (cooling) as distance is increased away from the FSE porphyry area.

deposition occurred. However, the immiscible vapor which separates from such a hypersaline liquid (Henley and McNabb, 1978), may have been absorbed into overlying meteoric water (Hedenquist and Arribas, 1994). Subsequent lateral outflow from the vicinity of the porphyry to the northwest then resulted in the observed cooling and dilution trend as recorded by the enargite fluid inclusions.

The fluid inclusions measured within enargite have consistent liquid-vapor phase ratios, and seem to record only syn-enargite deposition. Secondary inclusions from the quartz phenocrysts show multiple fluid events, but rarely trap fluids similar in character to their neighboring enargite hosted fluid inclusions. Data from the quartz phenocrysts also show a similar cooling trend but typically higher Th and lower salinity than the enargite hosted fluid inclusions. There are at least two possibilities to explain this difference. The first possibility is that the fluids are distinct in origin, the lower salinity, higher temperature fluid being earlier. The second alternative is that an early, lower salinity fluid cooled but had an increase in its apparent salinity, possibly caused by an increase in the dissolved gas content of the fluid (Hedenquist and Henley, 1985). This higher gas content was perhaps contributed by the underlying magma. A variation on this alternative could be that a high gas, low salinity parent fluid was present at depth throughout the evolution of the Lepanto system. In the early stage, the fluid boiled and lost much of its gas content, thus recording low apparent salinities. If boiling was quenched due to higher pressures and/or groundwater dilution, the gas content of the deep parent fluid would remain in solution, accounting for the high apparent salinity of the enargite mineralizing fluid.

CONCLUSION

The enargite-hosted fluid inclusions at Lepanto record a simple cooling and dilution trend away from the vicinity of the FSE porphyry Cu-Au deposit, the likely heat source of the epithermal high-sulfidation system. Although there is a large difference in fluid inclusion values between the porphyry and high-sulfidation epithermal mineralization at Lepanto, the close spatial and temporal relation between these areas suggests that the porphyry must have contributed components to the epithermal system possibly as a low-salinity vapor. It is likely that this vapor separated from the magmatic fluids of the porphyry and ascended to interact with the local groundwater which had a NE lateral flow component along the permeable Lepanto fault. Upon cooling and dilution of this fluid, enargite was deposited. It is probable that two distinct fluids produced the fluid inclusions found within the quartz phenocrysts and in the later enargite deposition, but a single fluid charged by a gas flux could produce the differences seen in the data sets by increasing a fluid's apparent salinity during cooling and dilution of the system.

REFERENCES

Arribas A, Jr., Hedenquist J.W., Itaya T., and Garcia J.S. Jr. (1994) Timing of intrusion and related porphyry and high sulfidation Cu-Au mineralization at Lepanto-FSE, Philippines. *Resource Geol.*, **44,** 266.

Burns R.G. (1970) Mineralogical applications of crystal field theory, Cambridge, Cambridge University press, 224 p.

Campbell A.R., Hackbarth C.J., Plumlee G.S., and Petersen U. (1984) Internal features of ore minerals seen with the infrared microscope. *Econ. Geol.* **79.** 1387-1392.

Campbell A.R. and Robinson-Cook, S. (1987) Infrared fluid inclusion microthermometry on coexisting wolframite and quartz. *Econ. Geol.* **82,** 1640-1645.

Campbell A.R. (1991) Geologic applications of infrared microscopy in C.E. Barker and O.C. Kopp (Eds.). *Luminescence microscopy: Quantitative and qualitative aspects, SEPM short course #25.* 161-171.

Claveria J.R. and Hedenquist J.W. (1994) Paragenesis of Au and related minerals in the Lepanto Cu-Au deposit. *Resource Geol.*, **44,** 267.

Concepcion R.A. and Cinco J.C., Jr. (1989) Geology of the Lepanto Far Southeast gold-rich porphyry copper deposit, Mankayan, Benguet, Philippines. *Proceedings of the 28th International Geological Congress.* 1-319--1-320.

Deen J.A. (1990) Hydrothermal ore deposition related to high-level igneous activity; a stable-isotopic study of the Julcani mining district, Peru. *University of Colorado, Denver Colorado, Ph.d dissertation*, 263 p.

Evelend A.J. (1905) A preliminary reconnaissance of the Mankayan-Suyoc mineral region, Lepanto, Philippine Islands: Bull. Phil. Mining Bureau #4; also in Far Eastern Review, v. III (1906).

Garcia J.S., Jr. (1991) Geology and mineralization characteristics of the Mankayan mineral district, Benguet, Philippines. *Geol. Surv. of Japan Report*, **277,** 21-30.

Goldstein R.H. and Reynolds T.J. (1994) Systematics of fluid inclusions in diagenetic minerals. Society for Sedimentary Geology. *SEPM short course #31*, Tulsa, OK. 199 p.

Gonzales A.G. (1959) Geology and genesis of the Lepanto copper deposit, Mankayan, Mountain Province, Philippines. *Ph.D. dissertation, Stanford University.* 102 p.

Haar L., Gallagher J.S., and Kell G.S. (1984) NBS/NRC Steam Tables: Thermodynamic and transport properties and computer programs for vapor and liquid states of water in SI units. Hemisphere Publishing Co. 9-15.

Hayba D.O., (1984) Documentation of thermal and salinity gradients and interpretation of the hydrologic conditions in the OH vein, Creede, Colorado (abs.): Geol. Soc. America Program with Abstracts, **14,** 489.

Hedenquist J.W., Simmons S.F., Giggenbach W.F., and Eldridge C.S. (1993) White Island, New Zealand, volcanic-hydrothermal system represents the geochemical environment of high-sulfidation Cu-Au ore deposition. *Geology*, **21,** 731-734.

Hedenquist J.W. (1994) Flux of ore forming metals from Arc-volcanoes, and the formation of high-sulfidation ore deposits. *7 th Geological Congress of Chile* , v. 2, 817-821.

Hedenquist J.W., Aoki M., and Shinohara H. (1994a) Flux of volatiles and ore-forming metals from the magmatic-hydrothermal system of Satsuma Iwojima volcano. *Geology*, **22,** 585-588.

Hedenquist J.W., Matsuhisa Y., Izawa E., White N.C., Giggenbach W.F., and Aoki M. (1994b) Geology, geochemistry, and origin of high sulfidation Cu-Au Mineralization in the Nansatsu District, Japan. *Econ. Geol.* **89,** 1-30.

Hedenquist J.W. and Arribas A. (1994) The Lepanto Far Southeast hydrothermal system, Philippines: Transition from porphyry to epithermal Cu-Au mineralization. *Resource Geol.*, **44,** 268-269.

Hedenquist J.W., and Henley R.W. (1985) Effect of CO_2 on freezing point depression measurements of fluid inclusions: Evidence from active geothermal systems and implications for epithermal ore deposition. Econ. *Geol* . **80,** 1379-1406.

Henley R.W. and McNabb A. (1978) Magmatic vapor plumes and ground-water interaction in porphyry Cu emplacement. *Econ. Geol.*, **73,** 1-20.

Lehlbach L. (1906) Mankayan-Suyoc mines and Abra River placers, Lepanto-Bontoc Province, Luzon: Far eastern Review, v. III.

Mancano D.P. and Campbell A.R. (1994) Microthermometry of enargite in the Lepanto, Philippines, high sulfidation Cu-Au deposit using infrared microscopy. *Resource Geol.*, **44,** 267-268.

Ohmoto H. and Lasaga A.C. (1982) Kinetics of reactions between aqueous sulfates and sulfides in hydrothermal systems. *Geochim. Cosmochim. Acta*, **46,** 1727-1745.

Ohmoto H. and Rye R.O. (1979) Isotopes of sulfur and carbon; in Barnes, H.L. (ed.) Geochemistry of hydrothermal ore deposits, second edition: John Wiley and sons, New York, 509-567.

Richards J.P. and Kerrich R. (1993) Observations of zoning and fluid inclusions in pyrite using a transmitted infrared light microscope ($\lambda \leq$ 1.9 μm). *Econ. Geol.* **88,** 716-723.

Ringenbach J.C., Stephan J.F., Maleterre P., and Beller H. (1990) Structure and geological history of the Lepanto-Cervantes releasing bend on the Abra River Fault, Luzon Central Cordillera, Philippines: *Tectonophysics*, **183,** 225-241.

Sasaki A., Arikawa Y., and Folinsbee R.E. (1979) Kiba reagent method of sulfur extraction applied to isotopic work: *Bull. Geol. Surv. Japan*, **30,** 241-245.

Sillitoe R.H. (1989) Gold deposits in western Pacific island arcs: The magmatic connection. *Econ. Geol.* Monograph 6, 274-291.

Sillitoe R.H. and Angeles C. A., Jr. (1985) Geological characteristics and evolution of a gold-rich porphyry copper deposit at Guinaoang, Luzon, Philippines. *Asian Mining '85*, Instn. Min. Metall., London. 15-26.

Steven T.A., and Ratté J.C. (1960) Geology and ore deposits of the Summitville district, San Juan Mountains, Colorado. *U.S. Geol. Surv. Prof. Paper 343*, 70 p.

APPENDIX A

SAMPLE INVENTORY

In total, 82 hand samples and drill core samples were collected underground at the Lepanto Mine between January and March of 1993. Table 2 shows all samples which were collected, with the headings on the table corresponding to the author's sample collection number, corresponding mine coordinate location, mine level relative to sea level (meters), and the mineralogy of samples used for fluid inclusion (F.I.) and/or stable isotope (S.I.) analysis (if any). The sample locations are shown on three plan view sample maps. These include fluid inclusion host locations (see appendix C), sulfur isotope host locations (see appendix D), and unused sample locations (figure 8).

Sample locations can be found by using the current mine coordinate system described below. This system is a grid relative to the Earth's latitude and longitude. The Lepanto mine coordinate key is shown in figure 9. Mine locations are specified with a number followed by a letter and another number (e.g. 95 A 4). A location on any of the plan view coordinate maps (fig. 8, 10, 13) can be found by matching the first number with the Y-axis of the grid. The Y-axis is composed of a number between -50 to 200. The letter which follows corresponds to the X-axis. The X-axis contains three groups of letters Including: 1) letters A-Z (standard alphabet); 2) letters AZ, BZ, CZ... etc. which have the suffix "Z" used for additions to the eastern parts of the mine; and 3) letters AW, BW, CW... etc. which have the suffix "W" used for later additions to the northwestern part of the mine. The exact location within the square described by X-Y space can be found using the last number of the sequence as shown in figure 9. Some samples were collected in areas which spanned over two or

more letter blocks. These samples are denoted by commas between the letters. Only two abbreviations are used in the following tables. XCN and XCS represent the words crosscut-North and crosscut-South respectively. All samples listed are kept with the geoscience department at the New Mexico Institute of Mining and Technology.

Table 2. Sample Inventory from Lepanto, Phlippines

Sample #	Location	Level	F.I. Host	S.I. Host
2.2.1	170 DZ 4	950		
2.2.2	165 IZ 1	950	enargite	enargite, pyrite
2.5.1	80 NO	1150		
2.5.2	70 N 3	1030	enargite	enargite
2.5.3	55 M	1030		
2.6.1	(-)15 CW 2	1030		
2.6.2	(-)10 BW 1	1030		
2.6.3	(-)15 CW 2	1030		
2.6.4	(-)10 CW 3	1030	enargite	
2.8.1	85 L	1100		
2.8.2	90 M 5	1100		
2.8.3	50 J 4	1070		
2.8.4	50 J 4	1070	enargite	enargite
2.9.1	115 T 5	1030		enargite
2.9.2	45 P 4	950	enargite	
2.11.1	125 EZ 2	680		
2.11.2	125 FZ 1	800		
2.11.3	100 X	900		
2.12.1	140 GZ	700	enargite	
2.12.2	140 GZ	680		
2.12.3	120 CZ 3	680		
2.13.1	175 CZ	900		
2.13.2	185 EZ	900	enargite	enargite
2.13.3	185 EZ	900		
2.16.1	50 R 4	950		
2.16.2	45 P 4	950		
2.16.3	45 P 4	950		
2.16.4	50 P	950		
2.16.5	50 P 1	950		
2.16.6	40 MN 5	1000		
2.18.1	175 S	1150		
2.18.2	20 C	1000	enargite	
2.18.3	125 FZ 1	680		enargite, alunite
2.18.4	100 T 2	800		
2.18.5	175 CZ	900		
2.19.1	135 N 2	1100		enargite
2.19.2	125 BZ 1	700	enargite	enargite, pyrite
2.19.3	135 N 1	1100	enargite	
2.19.4	100 K	1100		

Table 2. (cont'd)

Sample #	Location	Level	F.I. Host	S.I. Host
3.6.1	115 Q 1	1030		
3.6.2	125 EZ 3	950	enargite	
3.6.3	50 PQ 2	1000	enargite	
3.6.4	95 S	1030		
3.6.5	165 O	1200	quartz phenocrysts	
3.11.1	50 P	950		
3.11.2	45 P 4	950		enargite, pyrite
3.11.3	50 Q 1	950		
3.15.1	(-)20 DW 2	1030		enargite
3.15.2	(-)10 AW	1030		
3.16.2	45 P 5	980	quartz	
3.16.3	50 P	950		
3.17.1	175 CZ	900	pyrite, qtz. pheno.	
3.17.2	85 T	900		
3.17.3	170 TUV	1030		
3.19.1	140 GZ	680	quartz phenocrysts	enargite, anhydrite
3.19.2	140 HZ	680		
3.25.1	15 A 4	1000		
3.25.2	30 N	1070		
3.25.3	35 O	1030		
3.25.4	135 EZ XCS	850	enargite, qtz. pheno.	
3.29.1	70 L 1	1100		
3.29.2	40 P	1030		
3.29.3	100 P 4	1030		
3.29.4	110 T	1000		
3.29.5	110 T	950		
3.29.6	130 V 3	950		
3.30.1	12 M 3	1100		
3.30.2	90 O 5	1030		
3.30.3	120 N 5	1070		
3.30.4	160 Q 5	1150		
3.30.5	50 PQ	1100		
3.30.6	120 BZ 2	900		
4.2.1	120 S	1030	enargite	
4.2.2	(-) 5 A	1070		
4.2.3	30 J 4	1070		
4.2.4	15 G 1	1070		

Table 2. (cont'd)

Sample #	Location	Level	F.I. Host	S.I. Host
4.2.6	165 O	1200		
4.3.1	50 M 5	1030	enargite, qtz. pheno.	enargite, barite
4.3.2	95 T	1030	enargite	enargite
U.85.21	140 RZ 3	592	enargite	
U.86.3.A	145 XZ 2	353	vein quartz	

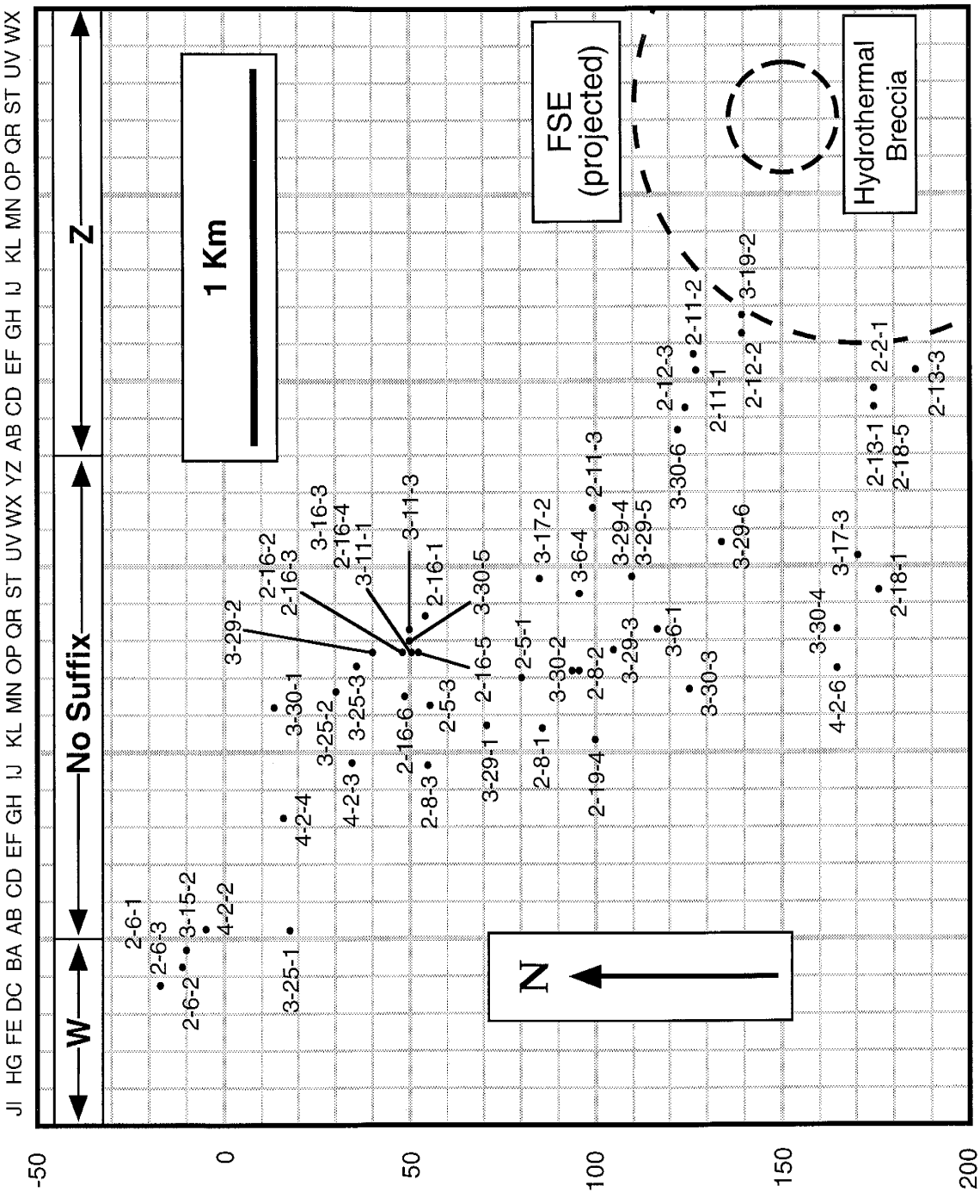

Figure 8. Plan view map of unused sample locations from Lepanto, Philippines

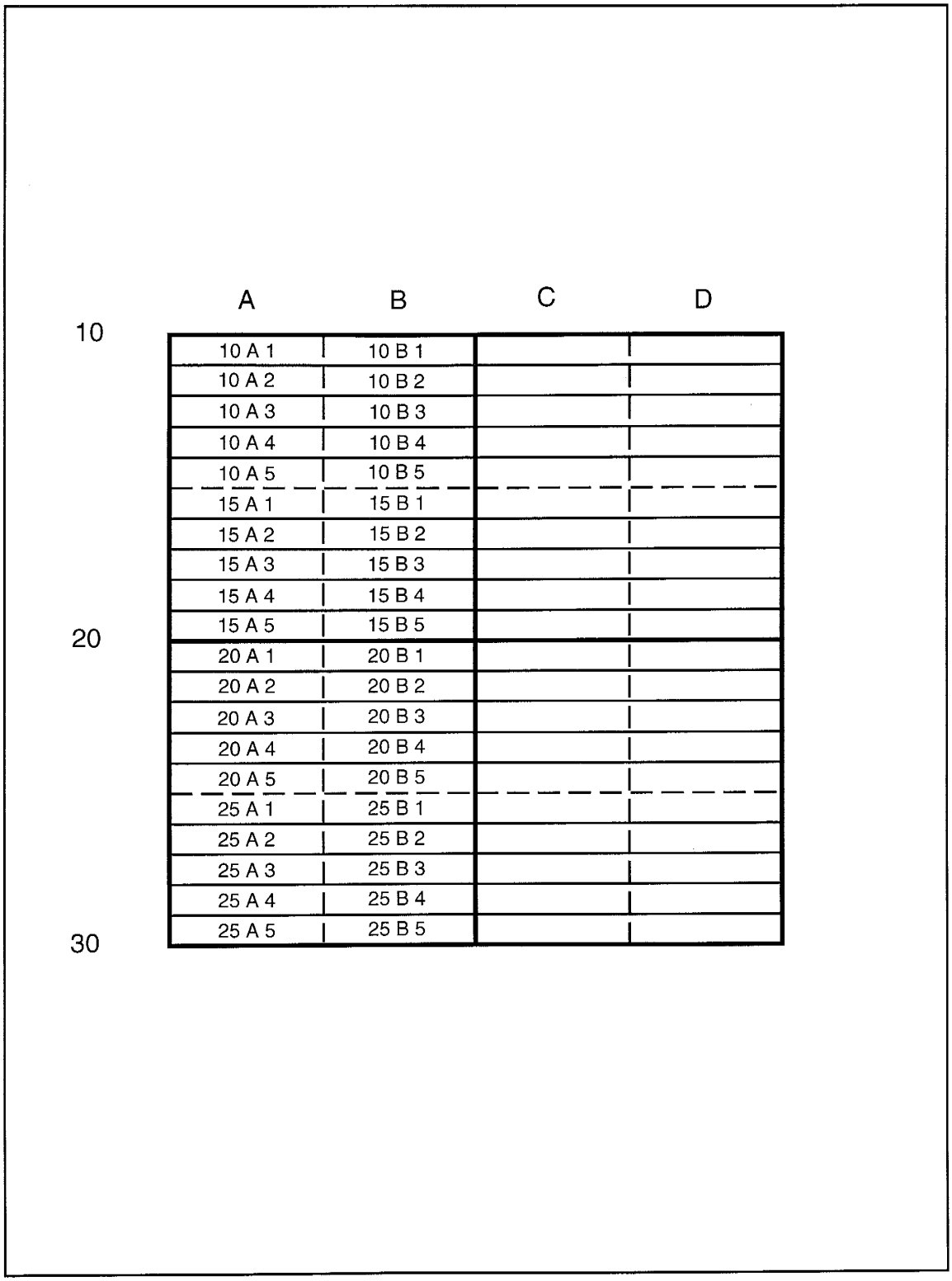

Figure 9. Lepanto mine coordinate key

APPENDIX B

SAMPLE PARAGENESIS

Sample paragenesis is described below for all samples which had either fluid inclusion microthermometry or sulfur isotopic analysis performed on them. Paragenesis is based on hand sample and microscopic (reflected light) observations. Descriptions are listed with the earliest occurring minerals described first.

Sample #	Description
2.2.2	Vug filling mineralization. Host not present. Luzonite and 1.0 cm, euhedral enargite / 0.5 cm, amorphous pyrite / minor anhedral enargite / 0.5 cm, euhedral pyrite.
2.5.2	Breccia ore mineralization. The silicified host rock contains disseminated pyrite. The host rock is brecciated, and the clasts (up to 7.0 cm) are coated with alternating, anhedral enargite and pyrite. The matrix is composed of 0.75 cm, subhedral-euhedral enargite. Minor, drusy quartz coats some enargite matrix. Minor pyrite coats the drusy quartz. A 0.5 cm wide anhedral quartz vein brecciates the matrix.
2.6.4	Breccia ore mineralization. The silicified host rock contains disseminated pyrite. The host rock is brecciated, and the clasts (up to 3.0 cm) are coated with minor, anhedral pyrite and enargite. Up to 0.75 cm subhedral-euhedral enargite also occurs as clasts with an anhedral quartz matrix. Some of the enargite clasts are being replaced by chalcopyrite.
2.8.4	Vug filling ore mineralization. The silicified host rock contains disseminated pyrite. 5.0 cm, euhedral enargite occurs in vug fillings. Minor pyrite "dusts" the enargite.

Drusy quartz (0.1 cm) and clay (kaolinite?) coat some of the enargite. Highly oxidized.

2.9.1 Open space filling ore mineralization. The silicified host rock contains disseminated pyrite. 1.0 cm luzonite / 0.5 cm, euhedral enargite. Kaolinite occurs in open spaces of the enargite.

2.9.2 Open space vein filling ore mineralization. Host not present. 0.1 cm, euhedral pyrite / 3.0 cm, euhedral enargite.

2.12.1 Breccia ore mineralization. The silicified host rock contains disseminated pyrite. The host rock is brecciated and contains clasts up to 3.0 cm. 1.0 cm, anhedral pyrite brecciates 0.5 cm, euhedral enargite. Anhedral quartz is in the open spaces of the pyrite. This quartz also brecciates some of the pyrite-enargite into 2.0 cm clasts.

2.13.2 Vein filling ore mineralization. The host rock is silicified. 3.0 cm, euhedral enargite. Drusy quartz occurs on the enargite and in open spaces. This quartz also brecciates the enargite.

2.18.2 Open space filling ore mineralization. No host present. 3.0 cm, euhedral enargite with luzonite (intergrown?). Drusy quartz coats enargite in open spaces, and crosscuts enargite as a 0.04 cm vein. Minor pyrite brecciates the

quartz and also occurs as a coating on the enargite.

2.18.3 Vein filling ore mineralization. The silicified host rock contains alunite. The host is crosscut by quartz veins (up to 1.5 cm wide) and by minor veins (up to 0.5 cm wide) of subhedral enargite and pyrite.

2.19.1 Open space filling ore mineralization. No host present. 3.0 cm, euhedral enargite. Minor, 0.1 cm subhedral pyrite and 0.02 cm, euhedral quartz occur in the open space of the enargite.

2.19.2 Open space filling ore mineralization. The silicified host rock contains disseminated pyrite and anhedral pyrite in the open spaces of the vuggy silica. 2.0 cm, euhedral enargite.

2.19.3 Open space filling ore mineralization. No host present. 4.0 cm, euhedral enargite. 0.1 cm, subhedral pyrite and minor drusy quartz occur in the open space of the enargite. Minor, 0.2 cm, euhedral barite also occurs in other open spaces of the enargite.

3.6.2 Open space filling ore mineralization. The host is pyritized and silicified. 2.0 cm, euhedral enargite. Minor, 0.02 cm, euhedral pyrite occurs as an overgrowth (and replacement?) of enargite. Drusy silica and kaolinite.

3-6-3	Unknown mineralization type. The host rock is silicified. 0.2 cm, subhedral-euhedral enargite intergrown with luzonite. Minor chalcopyrite crosscuts the enargite. Minor pyrite replaces the enargite.
3.6.5	Unknown mineralization type. The host is pyritized and silicified and contains quartz phenocrysts up to 0.8 cm. 0.1 cm, euhedral pyrite and 0.5 cm, euhedral barite occur in the open space of the host.
3.6.6	The host rock is chloritized and contains disseminated chalcopyrite and a silver-colored sulfide of unknown mineralogy. A 0.5 cm quartz vein, that contains minor anhydrite, crosscuts the host rock.
3.11.2	Open space vein mineralization. The host rock is silicified. 0.1 cm, euhedral pyrite / 2.0 cm, euhedral enargite. 0.1 cm, euhedral quartz occurs in the open space of the enargite.
3.15.1	Breccia ore mineralization. Breccia is the host. 1.0 cm, subhedral enargite clasts in a silica matrix.
3.16.2	The silicified host rock contains disseminated pyrite. 0.75 cm, quartz vein crosscuts the host. This quartz vein contains disseminated pyrite.

3.17.1 Vug filling open space ore mineralization. The silicified host rock contains 0.5 cm, quartz phenocrysts. The vugs contain 1.0 cm, euhedral pyrite and 1.0 cm, euhedral enargite.

3.19.1 Vein filling ore mineralization. The silicified host rock contains disseminated pyrite and 0.75 cm quartz phenocrysts. The host is crosscut by a vein containing the following minerals: 0.2 cm, anhedral pyrite / 0.4 cm, anhedral enargite / 2.0 cm, subhedral anhydrite. A second stage of anhydrite brecciates all of the phases.

3.25.4 Unknown mineralization type. The pyritized (80%) and silicified host rock contains 0.5 cm, quartz phenocrysts. Open space fillings in the host rock contain 0.1 cm, euhedral pyrite. Other open spaces contain 0.5 cm, euhedral enargite.

4.2.1 Unknown mineralization type. The host rock is silicified. 4.0 cm, euhedral enargite. Minor pyrite and quartz occur in the open space of the enargite

4.3.1 Open space vug filling ore mineralization. No host present. 5.0 cm, euhedral enargite. Minor chalcopyrite crosscuts the enargite. Drusy quartz and pyrite. Major, 1.0 cm, euhedral barite occurs in the open space of the quartz.

4.3.2 Breccia ore mineralization. Breccia is the host. 1.0 cm, euhedral enargite occurring as breccia clasts (and matrix?). Chalcopyrite crosscuts the enargite and coats the enargite clasts. Minor, 0.2 cm anhedral pyrite clasts. Silica brecciates the enargite and pyrite. Minor 0.2 cm, euhedral barite occurs in some of the breccia open space.

U.85.21 Breccia ore mineralization. Breccia is the host. 1.0 cm, subhedral enargite containing $\leq$ 25 μm, euhedral, hexagonal, translucent silicate inclusions. Covellite replaces 50% of the enargite. Chalcopyrite also replaces enargite. 0.5 cm, anhedral pyrite / 0.1 cm, euhedral anhydrite. A second stage of 0.2 cm, euhedral anhydrite brecciates the first anhydrite phase.

APPENDIX C

FLUID INCLUSIONS

All fluid inclusion data from enargite, pyrite, quartz phenocrysts, and quartz veins are shown in Table 3. The labels in table 3 correspond to sample number, mine location, mineralogy, inclusion type (P=primary, S=secondary), temperature (°C) of ice melting (Tm), Salinity (sal), temperature (°C) of homogenization (Th), and enthalpy (h). The plan view locations of the samples are shown in Figure 10, with the fluid inclusion data plotted in Th and Tm histograms (fig. 11 and 12). All fluid inclusion data was recorded from a USGS gas flow stage at the New Mexico Institute of Mining and Technology fluid inclusion laboratory. A four point calibration was carried out each month, and a zero point calibration was performed each day of sample analysis. This data is shown in table 4 with the date of calibration, type of standard, actual temperature (°C) of the standard, and observed temperature (°C) of the standard.

Table 3. Fluid Inclusion Data from Lepanto, Philippines

Sample	Location	Mineral	Type	Tm	Sal	Th	h
2.2.2	165 IZ 1 (950 lv)	Enargite	*	-1.4	2.4	249	1081
			*	-1.2	2.1	243	1052
			*	-1.3	2.2	242	1047
			*	-1.4	2.4	257	1120
			*	-1.5	2.6	Decrep.	*
			*	-2.0	3.4	250	1085
			*	-1.9	3.2	*	*
			P	-1.9	3.2	267	1169
			*	-1.5	2.6	250	1085
			*	-1.8	3.1	233	1004
2.5.2	70 N 3 (1030 lv)	Enargite	*	-1.7	2.9	*	*
2.6.4	(-)10 CW 3 (1030 lv)	Enargite	*	-1.2	2.1	*	*
			*	-1.1	1.9	*	*
			P	-1.0	1.7	196	834
			P	-0.9	1.6	157	663
			*	-0.9	1.6	169	715
			*	*	*	151	637
			*	*	*	162	684
			*	*	*	163	689
2.8.4	50 J 4 (1070 lv)	Enargite	P	-1.3	2.2	207	884
2.9.2	45 P 4 (950 lv)	Enargite	*	-1.5	2.6	<225	*
			*	-1.6	2.7	221	948
			*	-1.6	2.7	223	957
			*	-1.4	2.4	217	930
			*	-1.8	3.1	236	1018
			*	-1.6	2.7	193	821
			*	-1.5	2.6	238	1028
			*	-0.8	1.4	226	971
			*	-2.7	4.5	234	1009
			*	-2.5	4.2	233	1004
2.12.1	140 GZ (700 lv)	Enargite	P	-0.8	1.4	240	1037
			*	-0.3	0.5	168	711
			P	-1.7	2.9	*	*
			P	-0.8	1.4	249	1081
			P	-0.8	1.4	198	843
			*	-0.8	1.4	233	1004
			*	-1.3	2.2	245	1061
			*	-1.4	2.4	250	1085
			P	-1.4	2.4	259	1129
			P	-0.9	1.6	>240	*

Table 3. (cont'd)

Sample	Location	Mineral	Type	Tm	Sal	Th	h
2.13.2	185 EZ (900 lv)	Enargite	P	-1.6	2.7	245	1061
			P	-1.2	2.1	193	821
			P	-0.7	1.2	185	785
			*	-0.4	0.7	175	741
			P	-1.3	2.2	234	1009
			*	-1.8	3.1	>200	*
2.18.2	20 C (1000 lv)	Enargite	*	-1.7	2.9	202	861
			P	-2.1	3.5	190	808
			*	-1.6	2.7	209	893
			*	-1.6	2.7	195	830
			P	-1.4	2.4	214	916
			*	-2.2	3.7	207	884
			*	-2.2	3.7	207	884
			*	-0.5	0.9	187	794
			*	-0.5	0.9	173	732
			*	-0.6	1.1	197	839
2.19.2	125 BZ 1 (700 lv)	Enargite	P	-1.4	2.4	*	*
			*	-1.3	2.2	191	812
			P	-0.5	0.9	187	794
			P	-0.5	0.9	*	*
			P	-0.6	1.1	*	*
			*	-0.9	1.6	200	852
			*	-0.9	1.6	200	852
			*	-1.2	2.1	203	866
			*	-1.7	2.9	223	957
			*	-0.7	1.2	201	857
2.19.3	135 N1 (1100 lv)	Enargite	P	-1.3	2.2	203	866
			*	-0.9	1.6	210	898
			S	-1.5	2.6	207	884
			*	-0.8	1.4	225	967
			*	-0.9	1.6	241	1042
			*	-2.3	3.9	187	794
			*	-1.5	2.6	198	843
			*	-1.5	2.6	199	848
			*	-2.0	3.4	208	889
			*	-2.0	3.4	209	893
			*	-2.0	3.4	209	893

Table 3. (cont'd)

Sample	Location	Mineral	Type	Tm	Sal	Th	h
3.6.2	125 EZ 3 (950 lv)	Enargite	*	-1.3	2.2	251	1090
			*	-1.3	2.2	249	1081
			*	-1.1	1.9	>215	*
			*	-1.3	2.2	>200	*
			*	-1.2	2.1	254	1105
			*	-1.2	2.1	240	1037
			*	-1.5	2.6	247	1071
			*	-1.5	2.6	248	1076
			*	-1.5	2.6	247	1071
			*	-1.5	2.6	*	*
3.6.3	50 P, Q 2 (1000 lv)	Enargite	P	-2.0	3.4	Decrep.	*
			P	-0.4	0.7	197	839
			*	-0.9	1.6	244	1056
			*	-1.8	3.1	240	1037
			*	-1.9	3.2	232	999
			*	-1.3	2.2	225	967
			P	-1.0	1.7	245	1061
			*	-1.2	2.1	230	990
			*	-1.2	2.1	229	985
			*	-1.2	2.1	238	1028
3.6.5	165 O (1200 lv)	Quartz	S	-0.4	0.7	211	902
			S	-0.2	0.4	242	1047
			S	*	*	222	953
			S	*	*	250	1085
			S	-1.1	1.9	209	893
			S	-0.7	1.2	208	889
			S	-0.5	0.9	273	1200
3.17.1	175 CZ (900 lv)	Quartz	S	-0.6	1.1	253	1100
			S	-1.6	2.7	277	1221
			S	-0.2	0.4	281	1241
			S	-2.5	4.2	269	1180
			S	-0.4	0.7	270	1185
			S	-2.4	4.0	284	1257
			S	-2.4	4.0	282	1247
			S	-2.4	4.0	281	1241
			S	-2.4	4.0	279	1231
			S	-2.2	3.7	278	1226
			S	*	*	304	1367
			S	*	*	307	1384
			S	*	*	307	1384
3.17.1	175 CZ (900 lv)	Pyrite	P	-0.7	1.2	>120	*

Table 3. (cont'd)

Sample	Location	Mineral	Type	Tm	Sal	Th	h
3.19.1	140 GZ (680 lv)	Quartz	S	-0.7	1.2	337	1573
			S	-0.6	1.1	334	1552
			S	-0.7	1.2	351	1679
			S	-0.7	1.2	334	1552
			S	-0.6	1.1	324	1486
			S	-0.7	1.2	261	1139
			S	-0.9	1.6	242	1047
			S	-0.7	1.2	246	1066
			S	-0.2	0.4	329	1518
			S	-0.7	1.2	246	1066
3.25.4	135 EZ XCS (850 lv)	Quartz	S	-0.6	1.1	348	1654
			S	-0.6	1.1	363	1793
			S	-0.1	0.2	304	1367
			S	*	*	303	1361
			S	*	*	303	1361
			S	-0.2	0.4	348	1654
			S	-0.1	0.2	306	1378
			S	-0.1	0.2	297	1327
			S	-0.1	0.2	312	1413
			S	-0.7	1.2	291	1295
			S	-0.8	1.4	297	1327
			S	-0.8	1.4	291	1295
			S	*	*	322	1474
			S	*	*	307	1384
			S	*	*	289	1284
			S	*	*	297	1327
			S	*	*	298	1333
3.25.4	135 EZ XCS (850 lv)	Enargite	*	-1.4	2.4	*	*
			P	-1.0	1.7	196	834
			P	-1.0	1.7	187	794
			*	-1.0	1.7	183	777
			*	-1.7	2.9	244	1056
			P	-1.9	3.2	241	1042
			P	-1.4	2.4	*	*
			P	-0.8	1.4	238	1028
			*	-1.2	2.1	252	1095
			P	-1.2	2.1	>310	*
			*	-1.2	2.1	222	953

Table 3. (cont'd)

Sample	Location	Mineral	Type	Tm	Sal	Th	h
4.2.1	120 S (1030 lv)	Enargite	P	-1.8	3.1	230	990
			P	-1.9	3.2	230	990
			P	-1.3	2.2	203	866
			P	-2.0	3.4	215	921
			P	-1.7	2.9	236	1018
			P	-1.4	2.4	177	750
			P	-1.8	3.1	237	1023
			P	-1.9	3.2	229	985
			P	-1.9	3.2	231	995
			P	-1.2	2.1	232	999
			*	*	*	234	1009
			*	*	*	233	1004
4.3.1	50 M 5 (1030 lv)	Quartz	S	-1.0	1.7	179	759
			S	-1.0	1.7	215	921
			S	-1.0	1.7	220	944
			S	-1.1	1.9	233	1004
			S	-1.7	2.9	177	750
4.3.1	50 M 5 (1030 lv)	Enargite	*	-2.0	3.4	*	*
			P	-1.1	1.9	184	781
			P	-1.1	1.9	180	763
			P	-0.6	1.1	175	741
			P	-1.0	1.7	189	803
			*	-2.2	3.7	*	*
			*	-1.4	2.4	232	999
			*	-1.5	2.6	222	953
			S	-0.1	0.2	*	Decrep.
			*	-1.0	1.7	179	759
4.3.2	95 T (1030 lv)	Enargite	*	-1.6	2.7	213	911
			*	-1.1	1.9	219	939
			*	-1.3	2.2	217	930
			*	-1.6	2.7	215	921
			*	-2.1	3.5	215	921
			*	-2.0	3.4	185	785
			*	-1.3	2.2	*	*
			*	-2.3	3.9	190	808
			*	-2.3	3.9	190	808
			*	-2.2	3.7	216	925

Table 3. (cont'd)

Sample	Location	Mineral	Type	Tm	Sal	Th	h
U.85.21	140 RZ 3 (592 lv)	Enargite	*	-1.9	3.2	285	1262
			*	-1.9	3.2	281	1241
			*	-2.0	3.4	>200	*
			*	-1.9	3.2	294	1311
			*	-1.3	2.2	>260	*
			*	-1.1	1.9	>260	*
			*	-2.1	3.5	>250	*
			*	-1.2	2.1	>260	*
			*	-2.6	4.3	281	1241
			*	-2.6	4.3	>200	*
U.86.3A	145 XZ 2 (379 lv) (Cu-Au porphyry)	Quartz	P	*	68.0	>620	*
			P	*	68.0	>620	*
			P	*	68.0	>620	*

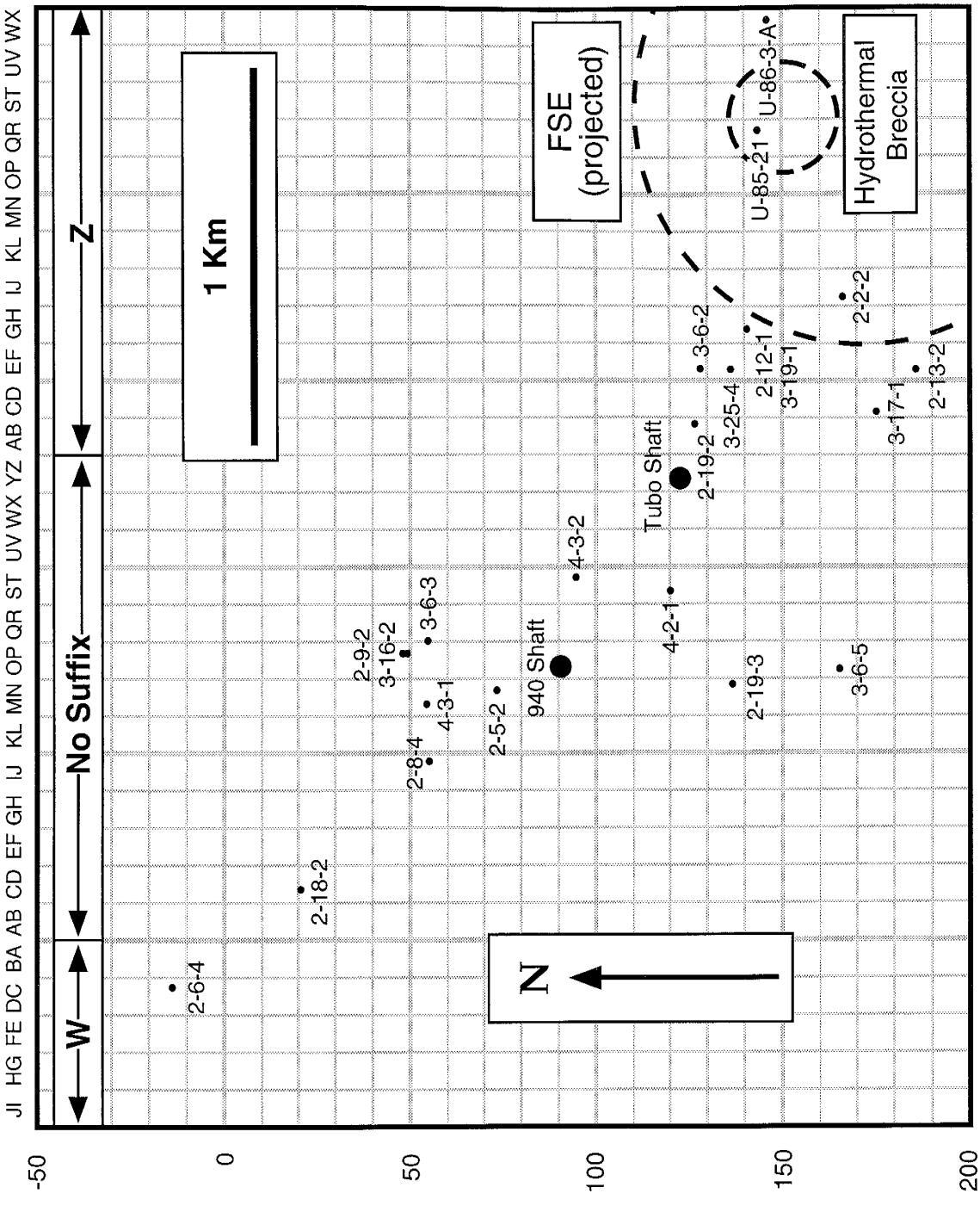

Figure 10. Plan view map of fluid inclusion-host sample locations from Lepanto, Philippines

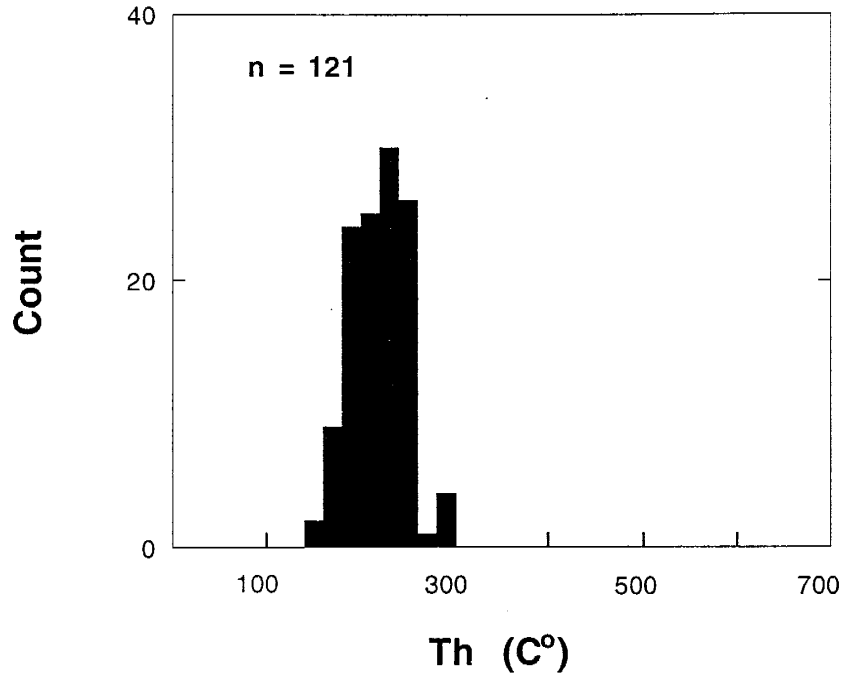

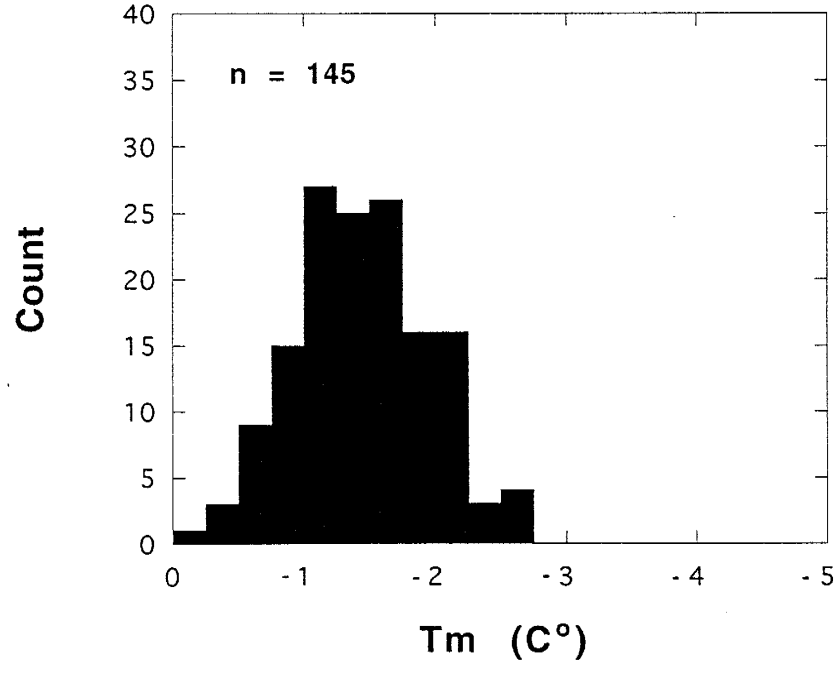

Figure 11. Th and Tm histograms of enargite-hosted fluid inclusions

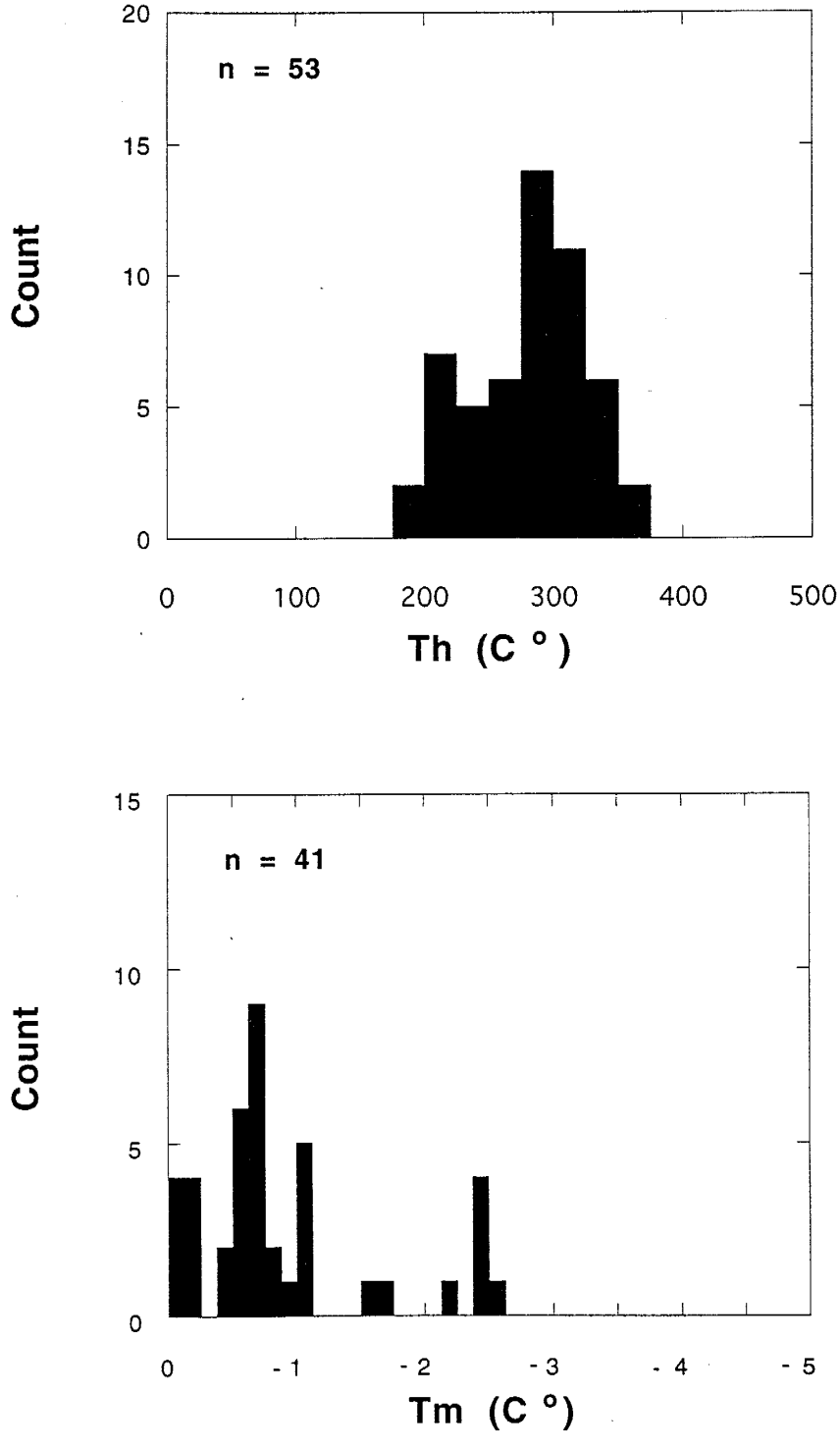

Figure 12. Th and Tm histograms of quartz phenocryst-hosted fluid inclusions

Table 4. Fluid inclusion heating/freezing stage calibration

Date	Standard	T actual	T observed		
2/3/94	CO2-H20	-56.6	-56.3	*	*
"	H2O	0.0	0.0	*	*
"	Acetanilid	114-116	114.4	*	*
"	Caffeine	235-237.5	237.3	*	*
"	AgCl	455	455.5	*	*
2/19/94	CO2-H20	-56.6	-56.5	*	*
"	H2O	0.0	0.0	*	*
"	Sulfapyridine	190-193	190.8	*	*
3/16/94	CO2-H20	-56.6	-57.0	-57.0	-57.0
"	H2O	0.0	-0.2	-0.2	-0.2
"	Sulfapyridine	190-193	191.8	191.5	*
3/19/94	H2O	0.0	0.0	0.0	0.0
"	CO2-H20	-56.6	-56.9	-56.8	*
3/20/94	H2O	0.0	0.0	*	*
3/21/94	H2O	0.0	-0.0	-0.0	-0.0
3/23/94	H2O	0.0	0.0	0.0	*
3/24/94	H2O	0.0	-0.0	-0.0	-0.0
3/26/94	H2O	0.0	-0.0	-0.0	*
3/27/94	H2O	0.0	-0.0	-0.0	*
3/30/94	H2O	0.0	-0.0	-0.0	*
3/31/94	H2O	0.0	-0.0	-0.0	*
4/2/94	H2O	0.0	-0.0	-0.0	*
4/3/94	H2O	0.0	-0.0	-0.0	*
4/7/94	AgCl	455.0	455.7	*	*
"	Sulfapyridine	190-193	192.8	191.6	*
"	H2O	0.0	-0.0	-0.0	*
"	CO2-H20	-56.6	-56.7	-56.7	*
4/8/94	H2O	0.0	0.0	-0.0	*
4/9/94	H2O	0.0	0.0	0.0	*
4/10/94	H2O	0.0	-0.1	-0.1	*
4/12/94	H2O	0.0	-0.0	-0.0	*
4/13/94	H2O	0.0	-0.0	-0.1	*
4/15/94	H2O	0.0	-0.0	-0.0	*
4/16/94	H2O	0.0	-0.1	-0.1	*
4/17/94	H2O	0.0	-0.1	-0.1	*
4/20/94	H2O	0.0	-0.1	-0.1	*

Table 4. (cont'd)

Date	Standard	T actual	T observed		
4/24/94	H2O	0.0	-0.1	-0.1	*
4/25/94	H2O	0.0	-0.1	-0.1	*
4/26/94	H2O	0.0	-0.0	-0.1	-0.1
4/30/94	H2O	0.0	-0.2	-0.2	*
5/1/94	H2O	0.0	-0.0	-0.1	*
5/3/94	H2O	0.0	-0.2	-0.2	*
5/4/94	H2O	0.0	-0.0	-0.0	*
5/6/94	H2O	0.0	-0.1	-0.1	*
5/8/94	H2O	0.0	-0.1	-0.1	*
5/9/94	H2O	0.0	-0.1	-0.1	*
5/10/94	H2O	0.0	-0.1	-0.1	*

A Guide to the Preparation of Enargite for Infrared Microthermometry

Introduction

The contents of this guide were developed over three years during fluid inclusion research of the opaque mineral enargite. Although the steps were designed for enargite, other opaque mineral studies will benefit from many of the ideas. However, each mineral is unique and may require different preparation steps to produce optimum results. It is hoped that the problems and setbacks encountered by the author are sufficiently addressed in this guide in hopes of increasing the efficiency of sample preparation in the future of infrared fluid inclusion microthermometry.

The goal of this guide is to provide the steps needed in taking a hand sample of enargite and producing a polished sample ready for infrared (IR) microthermometry. Due to the reduced clarity of the IR system, it is essential that every advantage be used to optimize image resolution. The most important of these advantages are well polished sample surfaces. The first section in this guide, *Preparation of Enargite Thick Sections*, will describe the grinding and polishing steps necessary to achieve the best possible polish of enargite. Due to the generally thin requirement of thick sections in IR studies, great care is required in the transition from petrographic slide to the heating/freezing stage. The second section, *Preparation for the Heating/Freezing Stage*, will address such problems and offer tips to ensure that samples are ready for analysis.

It is necessary to stress the importance of organization in the preparation of rock suites. When dealing with up to hundreds of samples, it is essential that a consistent and thorough labeling system is used throughout the preparation process. Because many splits of a sample result in the preparation process, it is necessary that all samples, slides, and holding containers are labeled. Samples should also be put away in a secure area so that other workers can not mix up unattended samples. The use of polishing equipment should be monitored closely to avoid abuse and contamination, and periodic inspection and replacement of the equipment should be carried out as needed. Being patient and keeping a clean organized area will ensure quality work and more comfortable working conditions.

Preparation of Enargite Thick Sections

Note: In preparation for a later stage of the procedure, prepare a box of petrographic glass slides by removing the polish on one side of each slide. A thin section machine provides a slide holder and a vertical polishing wheel of suitable grit to slowly grind away the glass surface. Also at this time, a container of super glue and an etching pen should be put aside.

1) Starting with a hand-sized specimen, trim the sample to fit on a standard petrographic glass slide using a water-cooled high speed saw. The thickness of the cut sample should be no more than ~2 cm. This cutting step should be used to produce the most homogeneous mineralogy possible throughout the cut sample. This will help to reduce contamination of the polishing medium from harder, neighboring minerals (sometimes this is not possible due to intergrowing and replacement textures).

2) The samples are now ready for grinding. Due to the use of high speed saws in the first steps, small scale microfracturing occurs on the sample edges adjacent to the saw blade (note the violent spalling and internal sparks that accompanies such cutting). These microfractures can break open fluid inclusions within the sample, thus ruining a once good host. This problem can be overcome by removing the affected area with a slow speed saw (see below) or a rough grinding wheel. The use of the grinding wheel is preferred since it combines the removal of the cutting material with the first rough grinding step.

Note: The actual grinding and polishing of the sample requires six to seven different wheels to produce the final polish. The first three to four wheels are for grinding and the last three wheels are for polishing.

Grinding

Grinding requires a large amount of water to flush off the wheel of cut debris so that small fragments (contaminant) do not scratch the sample face. For the grinding steps, adjust the water faucet (above the wheel) so that a "pencil thick" stream of water flows onto the center of the wheel. The wheel speed should be set at 500-1100 r.p.m. Adjust the speed to minimize plucking of the sample surface as well as contaminant residence time. Hold the sample between the thumb and first two fingers with the polishing face down. Keeping the sample face parallel to the grinding wheel, place the sample on the wet abrasive surface. Pressure on the sample should be the minimum amount required to produce abrasion. Using the wrist, continually turn the sample clockwise and counterclockwise while keeping the sample face parallel to the wheel. This action makes sure that cutting is not taking place in only one direction. It is also important to use the entire radius of the wheel so that preferential wear of the wheel surface does not take place. Preferential wear can lead to uneven or poor polishes, and will decrease the life of the wheel. A grinding time of ~30 seconds is usually adequate for each sample. More or less time may be required depending on the hardness of the sample.

Note: Let the wheel do the cutting. It is not necessary to use large arm movements or to rub the sample back and forth. Small wrist motions using the rotation method described above will help reduce arm fatigue, and ensure that the surfaces are flat.

- Using the polishing directions stated above, follow steps three through six. Always rinse off the sample with water between each step.

3) 75 μm metal-bonded diamond wheel. The primary goal in this first rough grinding step is to produce a flat surface for subsequent grindings.

Note: Steps four through six can be substituted using two metal-bonded diamond wheels. Equal results were found using both methods. The grinding technique is the same as described above.

4) 10 μm metal-bonded diamond wheel.

5) 30 μm resin-bonded diamond wheel.

6) 10 μm resin-bonded diamond wheel.

Polishing

The final three wheels are used in polishing the sample, and thus remove microscopic sized scratches which can hinder resolution during petrography and microthermometry. During the polishing steps, the sample surface is polished by the abrasive action of micrometer sized aluminum oxide particles suspended in water. It is very important to realize that the aluminum oxide suspension does the polishing, and that the nap of the wheel only prevents the loss of the polishing medium. Too much pressure on these polishing wheels will cause the nap to pluck the surface of the sample (usually seen as triangular cleavage marks in the enargite). Plucking contaminates the

aluminum oxide suspension and also ruins the flat surface of the sample. Therefore, it is essential that a constant cushion of water is maintained by initially wetting the nap of the wheel and providing a constant replenishment of aluminum oxide suspension and water as the sample is being polished. This is easily achieved by handling the sample in one hand, and replenishing the water and/or suspension with the other hand. If the wheel starts to grab the sample, add water. If the milky appearance of the aluminum oxide suspension can not be seen on the nap, add suspension.

Polishing does not require the constant flow of water used in the grinding steps. The wheel speed should be set at a lower 300-500 r.p.m. (adjust the speed to minimize plucking of the sample surface). With the polishing face down, hold the sample between the thumb and first two fingers. Keeping the sample face parallel to the grinding wheel, place the sample on the wet polishing surface. Pressure on the sample should be the minimum amount required to "float" the sample on the cushion of aluminum oxide suspension. Using the wrist, continually rotate the sample clockwise and counterclockwise keeping the sample face parallel to the wheel. A polishing time of ~30 seconds is usually adequate for each sample. More or less time may be required depending on the hardness of the sample .

If a grinding/polishing step is completed and scratches or a low spot are noticed, it may be necessary to go to a previous wheel to produce a new, flatter polishing surface. This problem can be lessened by constant visual inspection of the sample's polishing surface during and after each step. It is better to address these problems as soon as they occur since fixing mistakes is harder on the finer grit wheels. Since water hides scratches, it is of help to dry off the sample surface when examining it. Some paper towels may scratch the surface, but gentle blotting from a soft tissue is ideal.

Note: It is very important to avoid cross contamination of the polishing wheels. Liquid suspensions are easily contaminated, and foreign particles caught in the felt nap will ruin the polishing capability of the aluminum oxide suspension. In between polishing steps, always use water to spray off the sample and wash one's hands. This will insure that larger particles from a previous step do not get into the current suspension. Keep the wheels stored in a cabinet and spray them off with water before and after each day's work. Always thoroughly clean a wheel which is thought to have been contaminated. If the contamination is severe, replacement of the nap may be necessary.

Aluminum oxide suspension: Approximately two to three tablespoons of aluminum oxide powder should be placed in a 500 ml squirt bottle and mixed with water to produce a suspension which has a milky appearance (add powder as needed to create this appearance). These suspensions should be made starting with the 0.05 μm grit and ending with the 1.0 μm grit. This will help to prevent contamination of the source bottles.

- Using the polishing directions stated above, follow steps seven through nine. One should pay attention to the flatness and luster homogeneity of the sample face throughout the procedure.

7) 1.0 μm suspension on synthetic nap polishing wheel.

8) 0.3 μm suspension on synthetic nap polishing wheel.

9) 0.05 μm suspension on synthetic nap polishing wheel.

The first half of the thick section preparation is now complete. The polish on the sample should be mirror-like and homogeneous, with no visible streaks or cloudiness. Enargite will produce a black mirror finish in which one can see oneself. The highest degree of polish for each step will become evident to the polisher with experience.

The sample needs to be rinsed with water, and allowed to dry for ~15 minutes. During this time, one can etch the current sample's ID number into the polished side of a frosted slide. Once the sample is dry, apply two drops of super glue to the frosted side of the petrographic slide. Apply the flat, polished side of the sample to the slide. Once the sample is on the slide, gently move it back and forth with a gentle downward movement. This motion spreads the glue evenly and gets rid of air bubbles. It is important that the glue seeps around the perimeter of the sample so as to seal any spaces where the sample could be plucked off of the slide or where contaminants could get lodged during later steps.

Let the glue dry for ~30 minutes.

Note: The sample needs to be glued to a frosted slide to provide a footing for the epoxy, and to prevent peeling of the sample during the polishing steps. A smooth slide surface allows water under the epoxy layer, thus causing eminent peeling and microfracturing.

The sample now needs to be cut on a slow speed saw to reduce the thickness of the sample. Slow speed saws operate with water or oil based coolants. Oil coolant permeates the samples fractures and cavities and will later gum up the grinding/polishing wheels as well as hold contaminants on the sample. Therefore, the use of water based coolants is greatly preferred. The

polished side of the glass slide should be lightly greased with petroleum jelly so that the suction mechanism of the balancing-arm-sample-holder can work properly. The important points to remember when using a slow speed saw include: 1) using an unwarped, sharp, diamond saw; 2) providing only enough weight on the balancing arm to provide a positive downward pressure on the sample; and 3) starting an even cut of the sample to produce a flat polishing surface. This cut can be produced by slowly lowering the balancing arm until the sample touches the top of the blade. By repeating the raising and lowering of the arm in this fashion, one can produce a notch in which the blade can hold a straight cut through the sample. This is of great importance when the cutting surface of the sample is curved. One should never cut a sample on a slow speed saw by manually push-feeding the sample like many fast speed trim saw techniques. The blade is very thin and will break or bend easily.

Attach the slide to the balancing arm and use only enough weight and speed (~120 r.p.m.) to cut the sample.

The desired thickness of the sample is dependent on the experience of the polisher. However, on average, a sample thickness of ~1.0-1.5 mm is adequate.

After the sample has been cut, clean and dry off the leftover end piece and place it into a labeled sample bag. Take off the thick section from the sample holder and thoroughly clean off the glass slide of petroleum jelly to prevent grinding/polishing wheel contamination.

Moisten the polished side of the glass slide and place it on the lucite sample block. The sample will stay attached to the block with surface tension. This block allows the polisher to keep control of the thick section with a natural extension of the hand. Use the block the same way as prescribed in the *Grinding* section.

- Using the grinding directions stated above, follow steps three through six. One should pay attention to the flatness and luster homogeneity of the sample face throughout the procedure. If the sample thickness becomes uneven because of preferential material loss on one or two of its four sides (wedging), additional downward pressure can be placed on the side opposite the thinner side. This will create a new and even sample thickness.

Note: When working on the second side of the polished section, it is important to realize that the first and second grinding steps are the last steps which decide the actual thickness and general flatness of the sample. It is important that one does not cut off too much material or the section could be ruined.

The major differences in thick section preparation for the infrared system occur mostly in the second set of grinding/polishing steps. Infrared radiation transmission is a function of electronic mineral properties as well as thickness. A visually opaque sample could be transparent to the IR, but may be too thick. Because of this, it is suggested that when polishing the second side of a section, check the section's transparency before going on to the polishing steps. This will save a lot of time since only a moderate polish is needed to see the degree of transparency. With a 2.2 μm IR system, enargite samples are sometimes able to be cut to thicknesses of ~200 μm. Other samples may have to be reduced to ~50 μm. Because of the thin nature of some samples, the maximum size and quantity of fluid inclusions is reduced as the section becomes thinner.

- Using the polishing directions stated above, follow steps seven through nine. One should pay attention to the flatness and luster homogeneity of the sample face throughout the procedure.

While using the lucite block during the polishing steps, rinse the sample, sample block, and one's hands before each step due to the potential of trapping contaminants in the crevices of the block as well as under the slide.

Note: If polishing is being done as an exploratory study for a sample's transparency, It is sometimes beneficial to intentionally wedge the sample so that one edge is thinner than the other. By wedging the thinnest edge to the level of the glass slide, a continuum of increasing thickness is created across the sample. Upon inspection with the IR microscope, one can then determine if the sample is IR transparent, and at what thickness the transparency becomes prominent. This can speed up subsequent slide preparation and inventory characterization.

Upon completing the polishing steps, dry the sample thoroughly, and place it in a relatively air tight box so that oxidation of the surface (on polished sulfides) does not reduce the polish.

Preparation of Enargite for the Heating/Freezing Stage

To use the polished sample on the heating/freezing stage, the sample must be removed from the epoxy on the slide. The following guide explains the techniques and materials needed to successfully prepare a sample for transfer to the heating/freezing stage.

MATERIALS NEEDED

acetone	analytical spatula	weighing paper
Kim-Wipes (lint-free)	probe	ultra fine sharpie pen
3-petri dishes	thin rubber tube	glass cover slips
aluminum foil	tweezers	super glue
marking tape	q-tips	

Each labeled thick section should be placed in its own cleaned petri dish. Because the samples are so thin, they often break apart during the dissolution of the epoxy. This problem requires that the dish be initially clean (especially if the dish was used for a previous sample), and that the sample be by itself in the dish. The dish should be filled with acetone (covering the sample) and covered with aluminum foil. Mark the sample number on a piece of tape and place it onto the aluminum foil. The acetone bath should be allowed to dissolve the epoxy overnight.

Prepare a prefolded piece of weighing paper and exchange the adhesive sample label from the aluminum foil to the weighing paper. Set the weighing paper aside.

First, set aside a Kim-Wipe on a chemical resistant table top. Place a spatula under the glass slide and the sample and lift them both out of the petri dish. The sample should be floating free on top of the glass slide. Place the slide upside down (sample side down) on the Kim-Wipe, and slide the glass off of the sample.

Note: At this point, the sample is very delicate, and great care must be used in moving the sample around. Of greatest use during this procedure was a one foot long rubber tube with a 2.0 mm diameter opening and a removable pipet ending. By sucking on the end of the tube, one could lift and manipulate a thin sample far better than using tweezers or human fingers. The pipet end allowed the movement of very small fragments.

The sample must now be cleaned since the acetone bath will contain dissolved epoxy which will precipitate onto the drying sample. First use fresh acetone to lightly rinse the surface of the sample. Fold a portion of the Kim-Wipe onto the wet sample surface and allow the acetone to evaporate through the Kim-Wipe until the Kim-Wipe is dry. This will cause any residue to precipitate onto the Kim-Wipe. Repeat this rinsing and evaporation procedure until the sample surface comes clean. Thicker deposits might require the use of an acetone soaked Q-tip. Repeat the procedure for the opposite side of the sample. This technique is very effective and works well on small (~3mm), fragments which could not be cleaned otherwise. Using the suction tube, gently place the sample into the labeled, pre-creased weighing paper. Refold the paper so that the sample (or sample fragments) can not fall out, and store it in a safe place.

If the sample chips are too large for inclusion measurement, use a probe or razor blade to break apart the samples. This should be done inside of a clean, folded Kim-Wipe to prevent the chips from flying. As a rule, If a chip shoots out of the petri dish or weighing paper, it should not be used due to possible contamination from similar particles on the floor or desk top. Place approximately ten sample chips on a glass slide for petrographic analysis. Once a chip with measurable fluid inclusions is found, it must be determined whether or not the sample is thick enough to survive the pressure of the thermocouple and the force of the gas flow through the stage. If the sample is too thin it can be wafered between two cover glass slips with super glue acting as an epoxy around, but not touching the sample. This wafer should be labeled with a permanent marker. Wafering also provides a convenient method of storage and sample manipulation, but can adversely affect the optical quality of the fluid inclusion image (see below).

Image Enhancement Techniques for the 0.9-2.2 μm Olympus BHSM-IR Microscope

There are three different types of components which can be manipulated to improve image quality for IR microthermometry. These include: 1) sub-stage level components; 2) stage level components; and 3) super-stage level/external components.

Sub-Stage Level

The sub-stage level components consist of the transmitted light source and its condenser lens, and the second condenser lens, called the substage condenser. The transmission light source produces the infrared radiation which will pass through the opaque sample yielding an image. The transmission light source is a 12 volt, 100 watt halogen bulb which can have its intensity adjusted as needed. This light passes through a diaphragm and condenser which are housed in the base of the microscope. The diaphragm can be adjusted to let varying amounts of the light through. In almost all cases, the diaphragm is kept on its smallest diameter. This lets in a small, concentrated light source to the second condenser which lies above it. The second condenser is the substage condenser which contains a 50x IR objective. This objective is used to channel the transmission light source into a conoscopic area equal to the image-capturing area (~200 μm) of the objective above the sample. The matching objectives optimize the use of transmitted light by capturing all available light which passes through the sample. The substage condenser can be adjusted vertically to produce a variety of conoscopic light diameters down to 200 μm.

This small cone of concentrated light is quite adequate in illuminating an inclusion in the usually dark IR medium. The conoscopic light is also helpful in isolating an inclusion, thus preventing preferential heating of the heating/freezing stage thermocouple. Some inclusions on the edges of samples are washed out by extraneous light which passes around the edges. By placing a diaphragm on the surface of the first condenser, any diameter of conoscopic light can be produced on the sample. An easy handmade diaphragm can be created by punching a small hole (< 0.75 cm) in aluminum foil. The substage condenser can also be moved horizontally. This is of use when examining fluid inclusions with variable transparency and/or dark borders. The use of light offset to one side of the inclusion can often highlight previously opaque features. Some IR microscopes utilize varying wavelength IR filters to reduce the amount of extraneous visible light striking the bottom of the sample.

Stage Level

Stage level components consist of the heating/freezing stage and the sample itself.

The USGS gas flow heating/freezing stage uses a seven window system to contain the gas flow. These seven windows are high temperature silica windows or glass cover slips. Ideally, the high temperature silica glass windows should be used for there better optical qualities. The glass cover slips have marginal optical properties and it is suggested that the least flawed of these cover slips be chosen from a given supply. In either case, clean the surfaces with acetone to lessen any optical distortion caused by dirt and grease. Be careful when handling the silica glass windows as they are very expensive.

The sample must have a high polish. Polishing techniques are described in the previous section, *Preparation of Enargite Thick Sections*. The use of

cover glass slips as a wafering mechanism will decrease optical quality for the same reasons described above. Therefore, It is recommended to use wafering only when necessary.

Super-Stage Level

The super-stage level components consist of the objectives, IR camera, color video monitor, video printer, and the black and white monitor.

The BHSM-IR microscope has specially coated objective lenses to enhance image quality. These lenses are very expensive and should be handled carefully.

Always make sure 100% of the image is being directed to the camera and not partially to the microscope oculars. The IR camera controls are pre-adjusted and should not require any modifications.

The color video monitor shows the live image of the IR camera. The contrast, color, and brightness functions can be adjusted along with the substage optics to produce better contrast and resolution on difficult inclusions. The underscan function on a monitor flattens out the image of a curved monitor screen. This feature will produce a clearer picture.

The video printer captures a "frozen" image from the live feed and allows image manipulation (titles, graphics etc.) on the black and white monitor.

Note: Fluid inclusion microthermometry using an IR microscope commonly requires a cycling method to be performed on the Tm and Th measurements. Since ice is usually not visible during Tm, one must rely on the bubble morphology to determine if the fluid inclusion liquid phase is frozen. A still (room temperature) image placed next to the live image allows the experimenter a quick comparison of bubble size and shape during cycling. This morphology comparison can also be in Th cycling when the vapor phase starts to become small or is obscured by thick borders of the fluid inclusion walls.

Note: Due to the large output of all visible radiation from the 100 watt light source, the IR camera detector plate can be damaged if there is no opaque medium between the light source and the camera for prolonged periods of time. When there is no sample on the stage turn off the light source or move the objective out of the light path .

Equipment Cleaning

Use only filtered, canned pure air to remove dust off of the IR optical components of the microscope. Some halogen based aerosols cause damage to the coating on the IR optics. A more thorough cleaning of the optical surfaces can be achieved using ordinary lens cleaner and lens paper.

APPENDIX D

SULFUR ISOTOPES

Sulfur isotopes from samples representing all areas of mineralization (fig. 13) were analyzed by the author at the isotope laboratories of the Geological Survey of Japan. Sulfur was recovered from the samples with techniques utilizing the Thode and Kiba reagents method of sulfur extraction described by Sasaki et al., (1979). Silver sulfide produced using this technique was processed on a combustion type sulfur line and analyzed in a Finnigan Mat mass spectrometer dedicated to sulfur. Using the $\delta^{34}S$ of the samples (table 5), δH_2S fluid was calculated (Ohmoto and Rye, 1979, Ohmoto and Lasaga 1982) using known fluid inclusion Th values of the sample, or extrapolated Th for samples without fluid inclusion values. Since the fractionation factor for enargite is unknown, the fractionation factor of pyrite was used in the calculation of δH_2S for the enargite depositing fluid. Values for δH_2S (Fig. 14) show an average of -5.1‰ with a standard deviation of 2.9 ‰ and a range of -11.4‰ to +0.1‰.

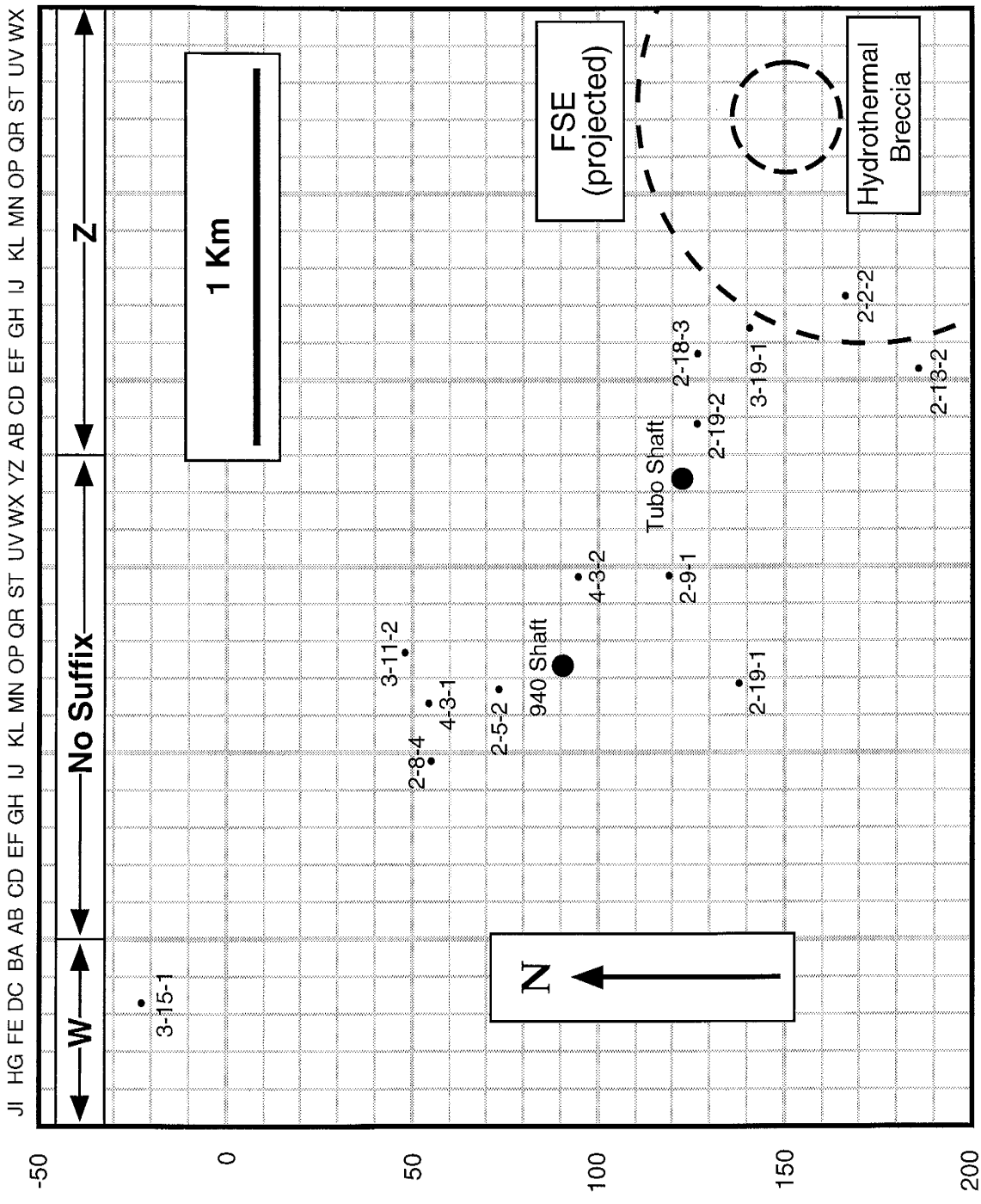

Figure 13. Plan view map of sulfur isotope-host sample locations from Lepanto, Philippines

Table 5. Sulfur Isotope data from Lepanto, Philippines

Sample #	Location	Level	Mineral	δ 34 S	δ 34 H_2S
2.2.2	165 IZ 1	950	Enargite	-2.6	-4.1
2.2.2	165 IZ 1	950	Pyrite	-0.8	-2.3
2.5.2	70 N 3	1030	Enargite	-7.2	-9.0
2.8.4	50 J 4	1070	Enargite	-9.7	-11.4
2.9.1	115 T 5	1030	Enargite	-1.6	-3.2
2.13.2	185 EZ	900	Enargite	-1.4	-3.1
2.18.3	125 FZ 1	680	Enargite	-1.7	-3.4
2.18.3	125 FZ 1	680	Alunite	+25.0	-2.7
2.19.1	135 N 2	1100	Enargite	-3.8	-5.5
2.19.2	125 BZ 1	700	Enargite	-7.4	-9.2
2.19.2	125 BZ 1	700	Pyrite	-5.1	-6.9
3.11.2	45 P 4	950	Enargite	-1.8	-3.4
3.11.2	45 P 4	950	Pyrite	+1.7	+0.1
3.15.1	(-)20 DW 2	1030	Enargite	-2.4	-4.5
3.19.1	140 GZ	680	Enargite	-1.0	-2.6
3.19.1	140 GZ	680	Anhydrite	+21.7	-3.8
4.3.1	50 M 5	1030	Enargite	-4.8	-6.6
4.3.1	50 M 5	1030	Barite	+23.0	-6.6
4.3.2	95 T	1030	Enargite	-6.8	-8.5

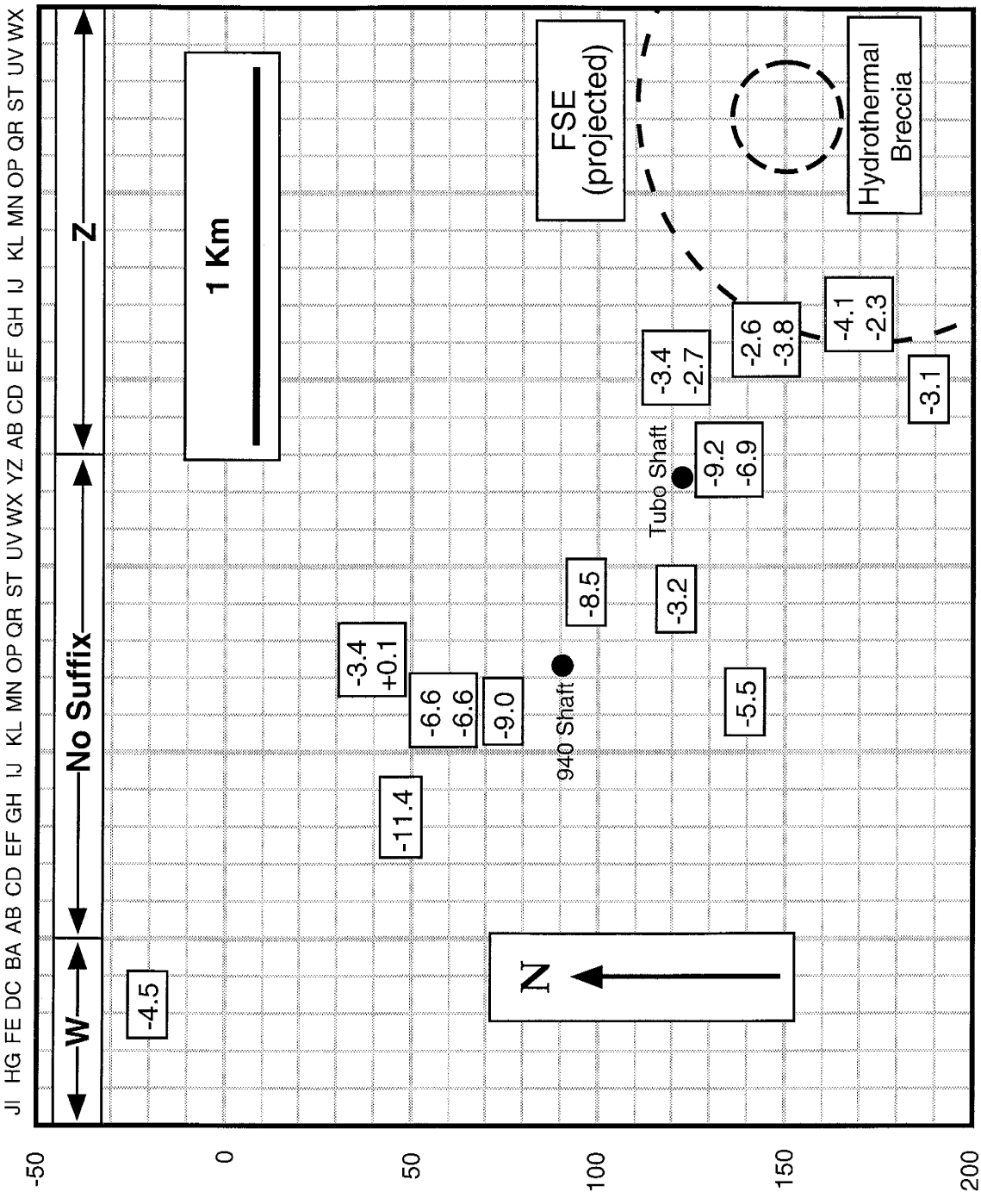

Figure 14. Plan view map of δH_2S-fluid values from Lepanto, Philippines

This thesis is accepted on behalf of the faculty of the Institute by the following committee:

Andrew Campbell

Adviser

David R. Noon

William X. Chávez, Jr.

12-15-94

Date